LIQUID METAL ION AND ELECTRON EMISSION STUDY

by

Gregory A. Schwind
B.A., Willamette University, 1974

A Thesis Submitted to the Faculty
of the Oregon Graduate Center
in Partial Fulfillment of the
Requirements of the Degree
Master of Science
in
Applied Physics

February 1977

This Master's thesis has been examined and approved by the following persons:

Lynwood W. Swanson
Professor
Thesis Research Advisor

Richard A. Elliott
Assistant Professor

Richard L. Pitter
Assistant Professor

ACKNOWLEDGMENTS

I would like to express my love and appreciation to my parents and sister for their continuing patience, love and support.

My sincere thanks go to my advisor, Dr. Lynwood Swanson, whose guidance and support throughout this work has been most valuable.

Special thanks go to Noel Martin and Gary Cabe for the technical support they provided.

I would also like to thank the members of my advisory committee, Drs. Richard Elliott and Richard Pitter for having seen me through my years of study at the Oregon Graduate Center, and to Bev Kyler for her speedy and efficient help in preparing the manuscript.

TABLE OF CONTENTS

LIST OF TABLES

LIST OF FIGURES

ABSTRACT

In this study an electrohydrodynamic technique was used to study both electron and ion emission from liquid Ga. This source proved to be very bright and capable of producing large total currents in either the electron or ion mode of operation. With ion emission three modes of operation were observed; the dc, high frequency, and the pulse mode. With electron emission only the pulse mode was obtained.

Three important factors in obtaining stable emission were the ability of the Ga to wet the nozzle, having the proper amount of Ga on the nozzle, and the source configuration. When these factors were satisfied, many hours of continuous and stable ion or electron emission could be obtained.

The actual emission mechanism is complex and is not fully understood. However, it appears to be initiated by field emission in the electron mode and field evaporation in the ion mode.

INTRODUCTION

A new type of electron and ion emission source is the liquid metal field emission source. An electrohydrodynamic (EHD) technique is used to generate either electrons or ions from a pointed emitter of liquid metal.

The technique involves feeding liquid metal to the tip of a small capillary tube (usually between .02 mm and .10 mm ID) and applying a voltage between the tip and an extractor electrode. The interaction of the electrostatic and surface tension forces causes the liquid metal meniscus to form a sharply peaked cone. The fields at the liquid metal-vacuum interface near the cone apex are sufficiently high to extract ions or electrons depending on the field polarity.

In recent years the EHD technique has been used to investigate ion emission from Ga,[1] Cs[2,3] and Ga-In[4] alloy. These studies show the EHD liquid metal ion source to have excellent potential as a high brightness ion source. Such a source would have valuable applications in areas of high density data storage, ion sputtering, microelectronics, and in microprobe work. Investigation of electron emission from liquid metals has only been briefly mentioned by Clampitt[2] in a Cs ion emission study report.

In this study the EHD technique was used to study both electron emission and ion emission from liquid Ga. For electron emission the

field emission model and for ion emission the field evaporation model are used to describe the liquid metal emission process. The actual process is complex and is not a pure field emission process. However, the liquid metal emission mechanism appears to be initiated by field emission for electron emission and by field evaporation for ion emission.

THEORETICAL CONSIDERATIONS

A novelty of liquid metal field emission source is that the emitter geometry is formed by the application of a high electrostatic field. It is hypothesized that the liquid metal forms a conical geometry where the electric field near the apex is sufficiently large to field evaporate ions. The formation of conical geometries when a liquid surface is subject to a high electric field has been experimentally demonstrated [4,5] and can lead to intense ion or electron emission depending on the voltage polarity.

For the liquid surface to exhibit a stable geometry it is necessary for the electrostatic stress, f_e, normal to the surface to be exactly balanced by the surface tension, f_s, forces. Taylor[5] has treated this problem in some detail.

The electrostatic stress and the surface tension forces are given respectively by

$$f_e = \frac{F^2}{8\pi} \tag{1}$$

$$f_s = \gamma_s \left(\frac{1}{\rho_1} + \frac{1}{\rho_2}\right) \tag{2}$$

where γ_s is the surface tension and ρ_1 and ρ_2 are the principle radii of curvature. For a sphere, infinitely long cylinder, and a cone Eq. (2) becomes respectively

$$f_s \text{ (sphere)} = \frac{2\gamma_s}{\rho} \tag{3}$$

$$f_s \text{ (cylinder)} = \frac{\gamma_s}{\rho} \tag{4}$$

$$f_s \text{ (cone)} = \frac{\gamma_s \cot\alpha}{r} \tag{5}$$

where ρ is the respective radii, and α is the half cone angle and r is the distance along the cone axis from the apex. Combining the above equations with Eq. (1), the conditions for equilibrium between the external electrostatic stress and the internal surface tension forces are

$$F \text{ (sphere)} = 4 \left(\frac{\pi\gamma_s}{\rho}\right)^{1/2} \tag{6}$$

$$F \text{ (cylinder)} = \left(\frac{8\pi\gamma_s}{\rho}\right)^{1/2} \tag{7}$$

$$F \text{ (cone)} = \left(\frac{8\pi\gamma_s \cot\alpha}{r}\right)^{1/2} \tag{8}$$

For the case of a cone, the angle α must be found such that $F \propto r^{-1/2}$. Taylor[5] showed that this occurred only if $\alpha = 49.3°$, in which case Eq. (8) becomes

$$F \text{ (cone)} = .93 \left(\frac{8\pi\gamma_s}{r}\right)^{1/2} \tag{9}$$

Most experimental studies have confirmed that the liquid surface under the influence of electrostatic forces forms a cone of half angle $\alpha \cong 49.3°$ as predicted. However, it is not known what actual geometry and radius the liquid surface assumes at the apex of the cone. This is of considerable interest because there exists no apparent theoretical reason to prevent the cone apex from forming the smallest

possible radius, i.e. one atom. The effect of a cone which approaches such an extremely small radius would be, as shown by Eq. (6) → (8), a very large electric field requirement at the apex.

Let us first consider a field electron emission model based on the Fowler-Nordheim equation[6] where the current density, J, is given by

$$J = 1.54 \times 10^{-6} \frac{e^{\frac{9.52}{\phi}}}{\phi} F^2 \, e^{\frac{-6.36 \times 10^7 \, \phi^{3/2}}{F}} \quad (A/cm^2) \tag{10}$$

where J is in Amperes/cm when F is in V/cm, and the work function ϕ in eV. The total current is then approximately given by

$$I = J\bar{A} \tag{11}$$

where $\bar{A}$ is the effective emitting area and can be approximated by cr^2, c a constant. Combining (6), (7) and (9) with Eq. (11), the total current as a function of radius, work function, and surface tension is given by

$$I \text{ (sphere)} = 6.96c \frac{e^{\frac{9.52}{\phi}}}{\phi} \gamma_s \rho \, e^{-2.99 \times 10^4 \, \rho^{1/2} \, \phi^{3/2} \, \gamma_s^{-1/2}} \quad (A) \tag{12}$$

$$I \text{ (cylinder)} = 3.48c \frac{e^{\frac{9.52}{\phi}}}{\phi} \gamma_s \rho \, e^{-4.23 \times 10^4 \, \rho^{1/2} \, \phi^{3/2} \, \gamma_s^{-1/2}} \quad (A) \tag{13}$$

$$I \text{ (cone)} = 3.01c \frac{e^{\frac{9.52}{\phi}}}{\phi} \gamma_s r \, e^{-4.54 \times 10^4 \, r^{1/2} \, \phi^{3/2} \, \gamma_s^{-1/2}} \quad (A) \tag{14}$$

These relations are correct for I in Amperes for r in cm, ϕ in eV and γ_s in dynes/cm. As shown by Figure 1 there is a fairly well defined range of radii values which produces total currents

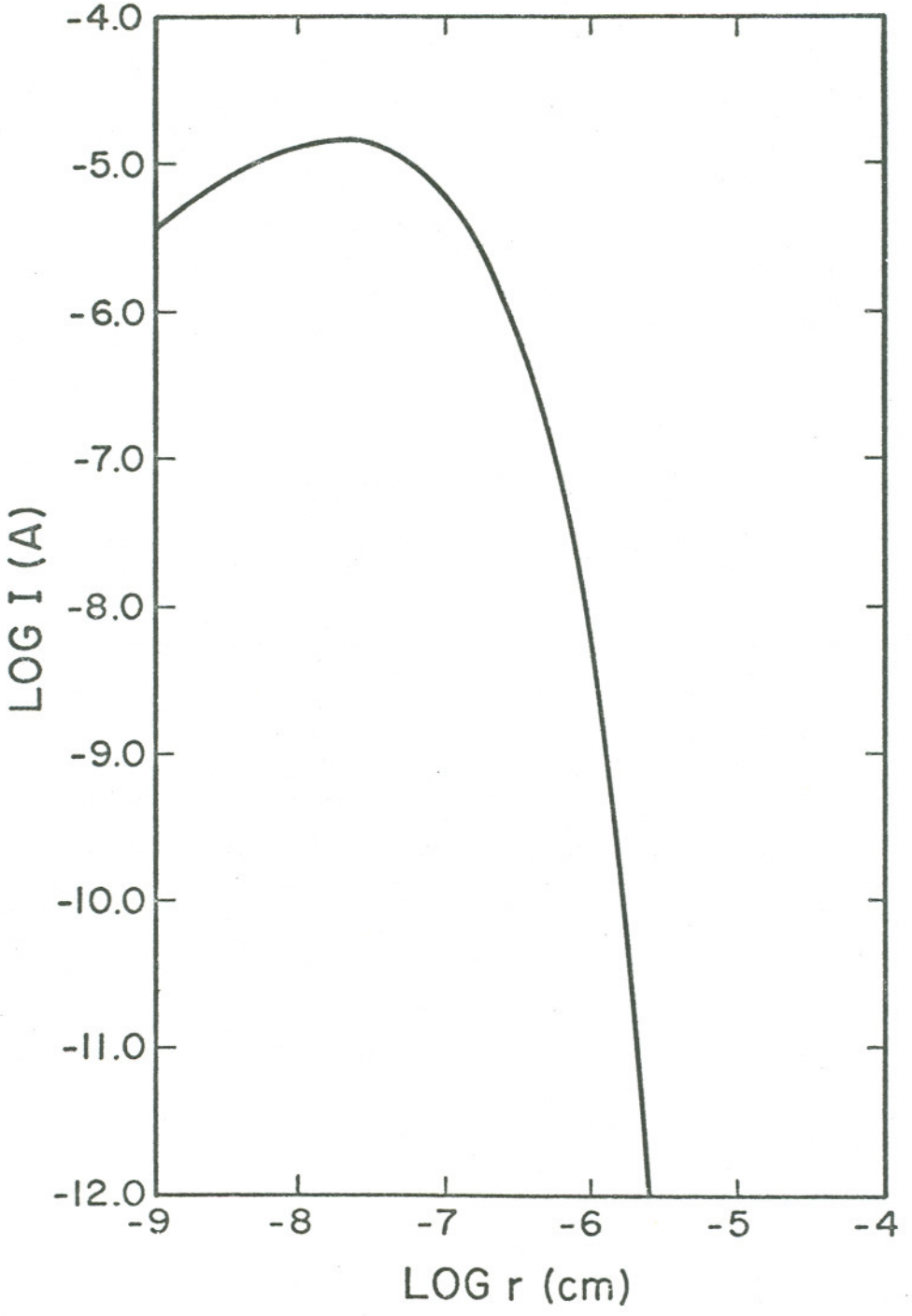

Figure 1. Plot of total current for a Ga cone vs radius based on Eq. 14 with c = 1.0.

approaching I_m, the maximum total current. The similarity of the previous equations indicate that results similar to Figure 1 should be obtained for a cone truncated by a spherical or cylindrical geometry. The radius, r_m, which produces I_m is only a function of surface tension and work function, and is given by

$$r_m \text{ (sphere)} = \frac{64\pi\gamma_s}{(6.36 \times 10^7 \ \phi^{3/2})^2} \tag{15}$$

$$= 4.47 \times 10^{-9} \ \frac{\gamma_s}{\phi^3}$$

$$r_m \text{ (cylinder)} = \frac{32\pi\gamma_s}{(6.36 \times 10^7 \ \phi^{3/2})^2} \tag{16}$$

$$= 2.23 \times 10^{-9} \ \frac{\gamma_s}{\phi^3}$$

$$r_m \text{ (cone)} = \frac{2.7\pi\gamma_s}{(6.36 \times 10^7 \ \phi^{3/2})^2} \tag{17}$$

$$= 1.93 \times 10^{-9} \ \frac{\gamma_s}{\phi^3}$$

where r_m is in cm when γ_s is in dyne/cm. Values of I_m/c and r_m are listed in Table I for several elements.

A comparison of Eqs. (7) and (9) reveals that the field required to stabilize a cylinder of radius ρ and a cone truncated at $r = \rho$ is approximately the same. This implies that a geometry which is a combination of a cone and cylinder is quite feasible. Some

experimental studies have reported a small cylindrical column extending from the cone apex.[5]

TABLE I

Values for several elements of r_m (Å) and I_m/c (μA) for sphere, cylinder, and a cone.

	Sphere		Cylinder		Cone	
Element	r_m	I_m/c	r_m	I_m/c	r_m	I_m/c
Cs	4.5	54	2.3	13	2.0	10
Rb	3.7	121	1.9	30	1.6	23
K	3.4	87	1.7	22	1.5	16
Na	7.8	430	3.9	108	3.4	81
Ga	4.7	81	2.7	20	20	15
Hg	2.3	18	1.2	4.7	1.0	3.5

If an anode is a distance R from the surface of the sphere, cylinder and cone, the voltages required to satisfy the conditions of Eq. (6), (7) and (9) are

$$V \text{ (sphere)} = \rho^{1/2}\, 4(\pi\gamma_s)^{1/2}\, (1 - \rho/R) \qquad (18)$$

$$= 2.13 \times 10^3\, \gamma_s^{1/2}\, \rho^{1/2}\, (1 - \rho/R)$$

$$V \text{ (cylinder)} = \rho^{1/2}\, (8\pi\gamma_s)^{1/2}\, \ell n\, \rho/R \qquad (19)$$

$$= 1.5 \times 10^3\, \gamma_s^{1/2}\, \rho^{1/2}\, \ell n\, \rho/R$$

$$V \text{ (cone)} = 1.4 \times 10^3\, \gamma_s^{1/2}\, R^{1/2} \qquad (20)$$

where V is in volts, γ_s in dynes/cm and ρ in cm. According to Eq. (20) the anode voltage required to stabilize a liquid cone depends only on γ_s and R. For Cs, Rb, K, Ga and Hg the required anode voltages for R = 1 mm are 3.4, 3.9, 4.11, 12.0, and 9.7 kV respectively.

Colby and Evans[7] have reported that the achievement of stable ionization was critically dependent on the relative position of the liquid cone and the anode. To examine the effect of the source configuration and relative anode position, the equipotential lines of the electrical field were calculated. Since the liquid surface can be considered as an equipotential line, the most desirable source configuration and anode position is that which results in the equipotential lines near the source forming a conical geometry of half angle $\alpha = 49.3°$.

To obtain the potential function, $\phi(r,z)$, it was necessary to solve, with the appropriate boundary conditions, Laplace's equation. For a function, $\phi(r,z)$ satisfying Laplace's equation in cylindrical coordinates,

$$\frac{\partial^2\phi}{\partial r^2} + \frac{1}{r}\frac{\partial\phi}{\partial r} + \frac{\partial^2\phi}{\partial z^2} = 0 \qquad (21)$$

the following relations hold:

$$\phi(r,z) = \frac{1}{4}\left[\phi(r,\ z+h) + \phi(r,\ z-h) + \phi(r+h,\ z) + \phi(r-h,\ z)\right] + \frac{h}{8r}\left[\phi(r+h,\ z) - \phi(r-h,\ z)\right] + O(h^4) \qquad (22)$$

$$\phi(o,\ z) = \frac{1}{6}\left[\phi(o,\ z+h) + 4\phi(h,\ z) + \phi(o,\ z-h)\right] + O(h^4) \qquad (23)$$

where h is the step size. Based on these relations, an iterative procedure and a Prime computer was used to calculate $\phi(r, z)$, and thereby the equipotential lines. The programs used are in Appendix I.

Typical results are shown in Figure 2. The relative anode position had no effect on the shape of the equipotential lines near the source. This is rather contrary to the claims of critical importance of the anode position for stable ion emission made by Colby and Evans.[7] As expected, the density of the equipotential lines, or alternatively the intensity of the electric field, near the source increased as the distance between the source and anode decreased. For all source configurations, the equipotential lines closely paralleled the source configuration boundaries. Thus, based on this data, a very favorable source configuration is shown in Figure 9(d), where the inserted emitter's tip is a cone of half-angle $\alpha = 49.3°$ and the liquid cone is formed on the point of the emitter.

Let us next consider ion emission from liquid metals based on a field evaporation model. The field required for field evaporation, assuming singly charged ionic species being emitted, is approximately given by the following expression[3]

$$F_{FE} = e^{-3} \left(H_{vap} + I - \phi - kT \ln \frac{\tau}{\tau_o} \right)^2 \qquad (24)$$

or

$$F_{FE} = .069 \left(H_{vap} + I - \phi - kT \ln \frac{\tau}{\tau_o} \right)^2 \ (V/\mathring{A})$$

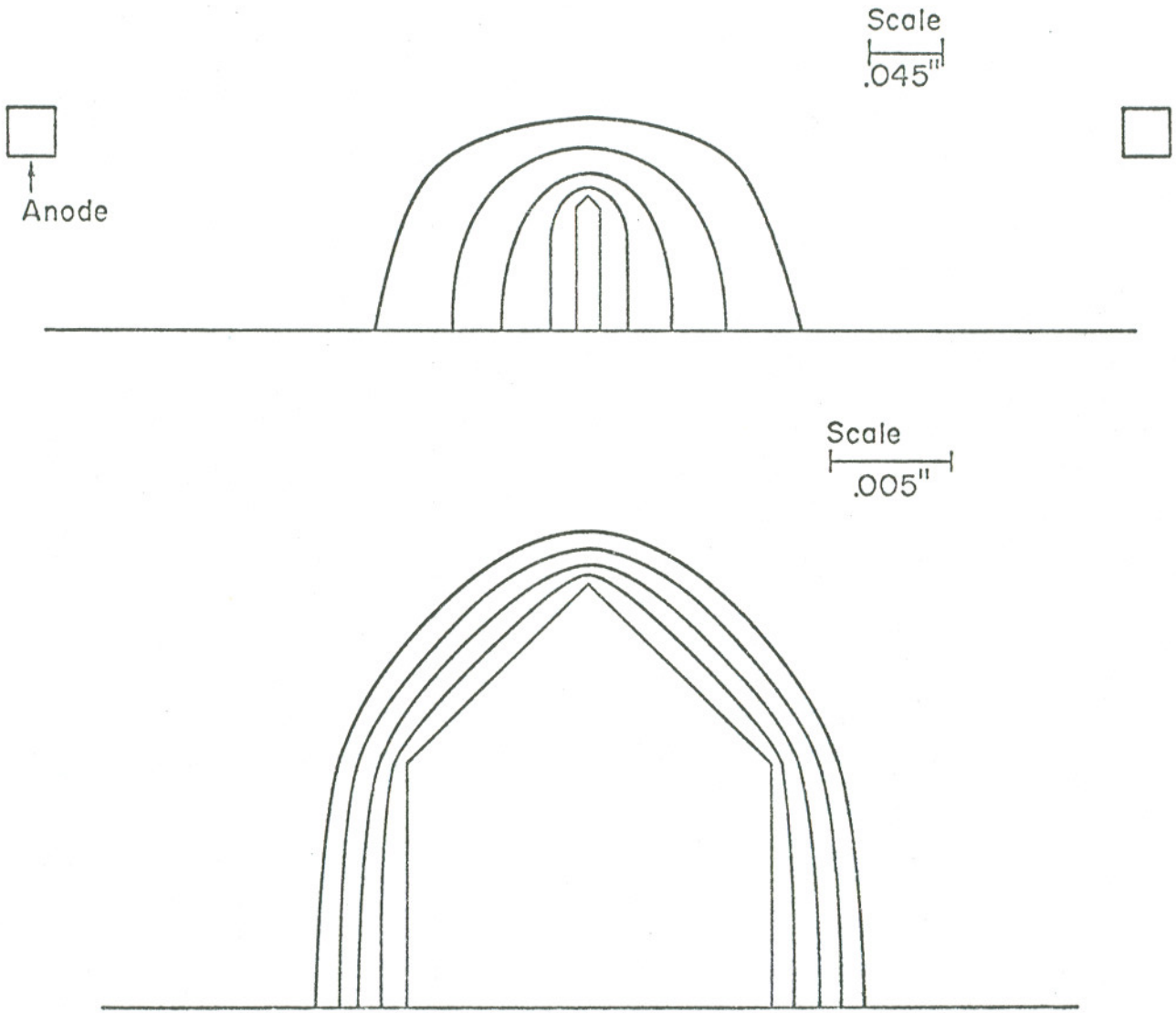

Figure 2. Calculated Equipotential Lines

where H_{vap} is the heat of vaporization, I, the ionization potential, τ, the lifetime in respect to field evaporation and $\tau_o \cong 10^{-12}$ sec. The second expression is correct for H_{vap}, I, kT and ϕ in eV and F in V/Å. The maximum radius, r_{vap}, of a conducting liquid cone where the evaporation fields have the required magnitude for atomic ion emission is easily obtained by substituting values of F_{FE} into Eq. (9). Values of r_{vap}, F_{FE} at 300°K, and other relevant parameters for several liquids are listed in Table II.

TABLE II

Evaporation Fields For Ion Emission From Liquids

Element	Vaporization Energy H_{vap} (eV)	Ionization Potential I (eV)	Work Function ϕ (eV)	Surface Tension γ (dyn/cm)	Evaporation Field F_{FE} (V/Å)	Evaporation Radius r_{vap} (Å)
Cs	.81	3.87	1.81	60	.36	10.5
Rb	.85	4.16	2.09	76	.32	16.8
K	.93	4.32	2.24	86	.40	12.1
Na	1.12	5.12	2.28	206	.78	7.7
Ga	2.82	5.97	4.12	735	1.14	12.8
Hg	.64	10.39	4.53	480	2.44	1.8

Small charged droplets, rather than ions, are in some cases emitted from the cone. Mahoney et al[3] concluded that ion, as opposed to droplet, formation will occur if the tensile strength of the liquid is large compared to the electrostatic stress required for field

evaporation, i.e. f_t/f_e is large. The theoretical tensile strength of a liquid column can be estimated by

$$f_t = 2\gamma_s/r_o \tag{25}$$

where r_o is the interatomic spacing. Mahoney, et al,[3] have tabulated values of r_o, f_t, and f_e which are reproduced in Table III.

TABLE III

Ratio of surface electrostatic stress at ion evaporation field strengths to theoretical stresses necessary to rupture a liquid column

Element	Interatomic Distance r_o (Å)	Tensile Strength $f_t \times 10^{10}$ (dyn/cm^2)	Electrostatic Stress $f_e \times 10^{10}$ (dyn/cm^2)	Force Ratio f_t/f_e
Cs	5.31	.226	.0545	4.15
Rb	4.97	.307	.0428	7.15
K	4.70	.365	.0691	5.28
Na	3.70	1.12	.263	4.26
Ga	2.77	5.3	.562	9.43
Hg	3.07	3.14	2.57	1.22

A favorable material for liquid field evaporation and field electron emission should possess a large f_t/f_e force ratio, be a conducting liquid at room temperature, and have a large H_{vap} value or alternatively a low vapor pressure. The latter property limits the gas phase electron impact ionization of the material during

electron emission and limits the gas phase ionization during ion emission.

EXPERIMENTAL

Several apparatus designs were tried for liquid field emission studies with each succeeding apparatus being an improvement of the previous. Each design has the flexibility to make the extractor and screen either positive or negative high voltage enabling both electron and ion emission to be studied. Figure 3 gives a cross-sectional representation of the initial apparatus tried. The plunger, controlled by a very sensitive differential screw micrometer drive, was expected to provide the delicate control necessary to adjust the position of the liquid metal meniscus at the top of the nozzle. The procedure was to attach the apparatus in a horizontal position to an ion pump vacuum system, put small solid chips of solid metal into the reservoir area, attach the plunger control system, pump the system down to $\approx 10^{-7}$ torr, melt the solid metal with the heating coils, force the liquid metal through the nozzle, check for emission. In all the experiments a binocular microscope was used to observe the nozzle.

The metal being used was Ga. It was chosen because of its low melting point (29.78°C), its very low vapor pressure (10^{-8} torr at 550°C), relative high f_t/f_e force ratio, and relative high wetting coefficient.

Trapped pockets of air in the liquid Ga reservoir and the inability of the liquid metal to wet the tip, prevented the plunger system from providing adequate control of the liquid Ga. The

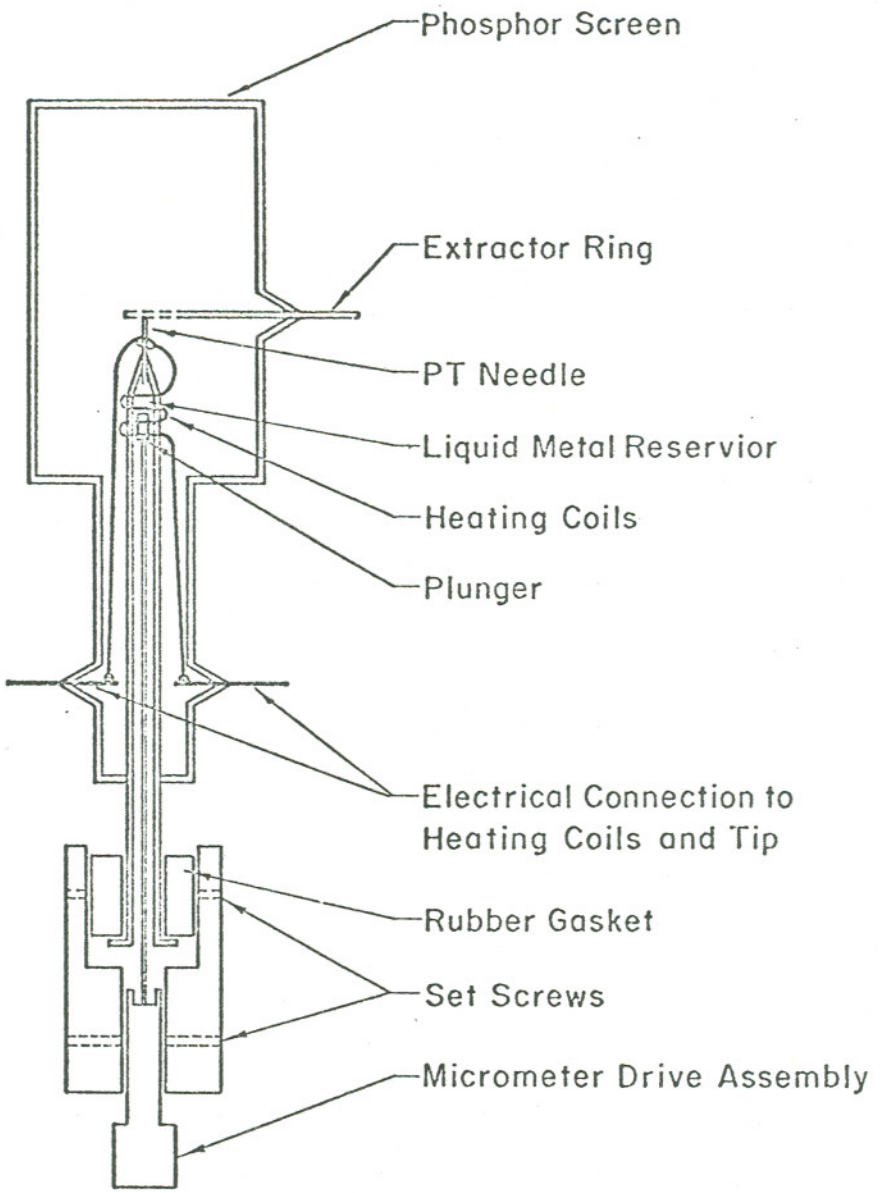

Figure 3. Diagram of initial apparatus used to study liquid Ga electron and ion emission.

majority of the time, droplets of liquid Ga, separated by air pockets, would drop off the tip of the nozzle. Occasionally a drop of liquid Ga could be positioned on the tip and in attempts to obtain field emission, an applied voltage of 5-6 kV (positive or negative) would provide sufficient electrostatic forces to pull the non-wetting liquid Ga off the tip. The experiments with this apparatus ended when the liquid Ga amalgamated with the plunger causing the plunger shaft to break.

Figure 4 shows the second apparatus used, with the major changes being the replacement of the plunger control system with a gas pressure control system and the ability to leak argon into the main vacuum chamber to enable ion sputter cleaning of the nozzle. The gas control system allows the same procedure as used previously to be followed, except when the system is pumped down, it is pumped from both the emission chamber side and the control system side, thus eliminating trapped air in the liquid Ga reservoir. To force the liquid Ga through the needle the valves connecting the mechanical vacuum pump and argon gas reservoir are adjusted to create a positive pressure difference.

Using the Laminar Force Equation,

$$Q = \frac{\pi}{8} \frac{R^4}{\eta} \frac{P_1 - P_2}{L} \tag{26}$$

where Q is the flow rate of a liquid, with viscosity η, through a tube of inside diameter R and length L. A simple calculation shows

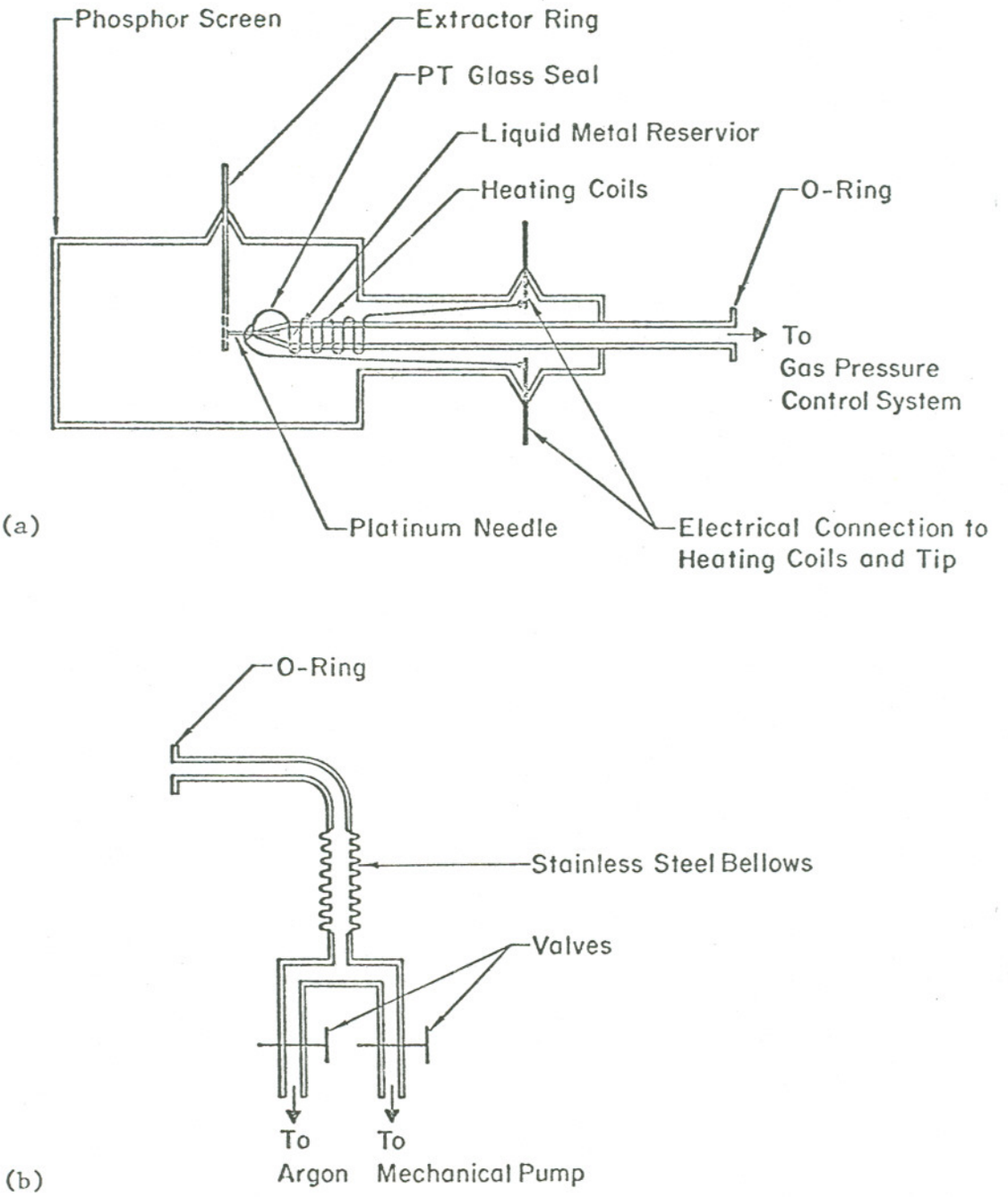

Figure 4. Diagram of emission chamber and liquid Ga source (a) modified to accept the gas pressure control system (b).

that .1 Atm pressure difference is sufficient to force liquid Ga through the Pt needle.

Upon melting the Ga chips, it was discovered each chip formed a sphere with a tough oxidized outer skin. A pressure difference of 2 atm was insufficient to break the skin and force the liquid Ga through the nozzle. Thus it became necessary to protrude a wire into the liquid Ga reservoir and break the oxidized skin on the spheres to form a movable reservoir.

Now, by applying a positive pressure difference, the liquid Ga could be forced through the Pt tubing. However, accompanying the positive pressure difference, was an increase in the main vacuum chamber pressure, often sufficient to cause the ion pump to turn itself off. Since the tube was filled with liquid Ga, this indicated an air leak from the pressure control system side into the main vacuum chamber. A careful inspection revealed the probable leak source as being the Pt to glass seal. This was no surprise, since Pt and glass make a poor seal.

To aid the liquid metal in wetting the nozzle, it was cleaned by argon in sputtering. Using the circuit shown in Figure 5, the nozzle was sputtered for several minutes by applying a negative voltage of 500-600 V to the needle in .05-.10 atm of argon. The current averaged approximately 200 μA. The sputtering definitely aided the liquid Ga in wetting the tip. This accomplished two things: (1) created greater ability to control position of liquid

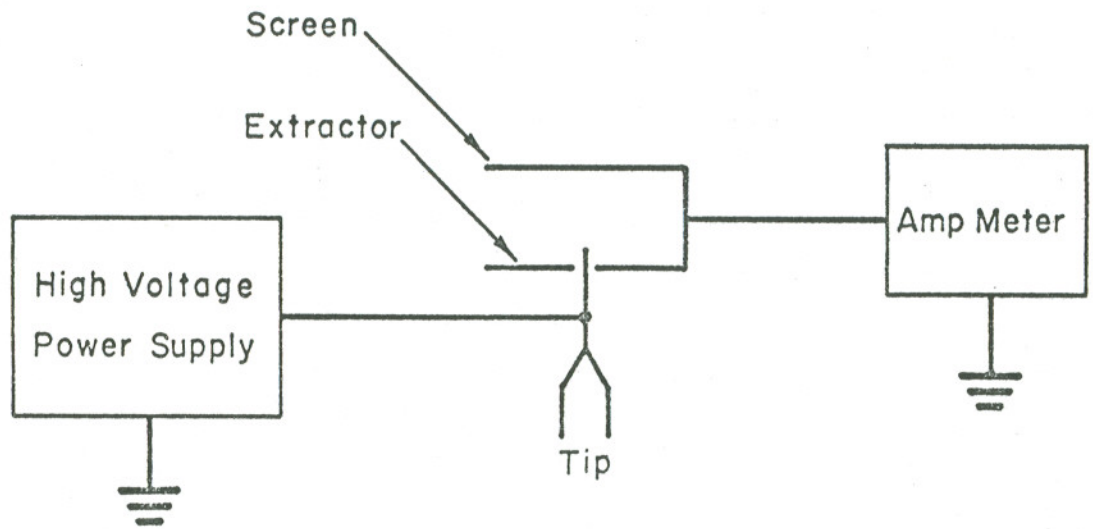

Figure 5. Circuit employed to argon ion sputter clean the needle.

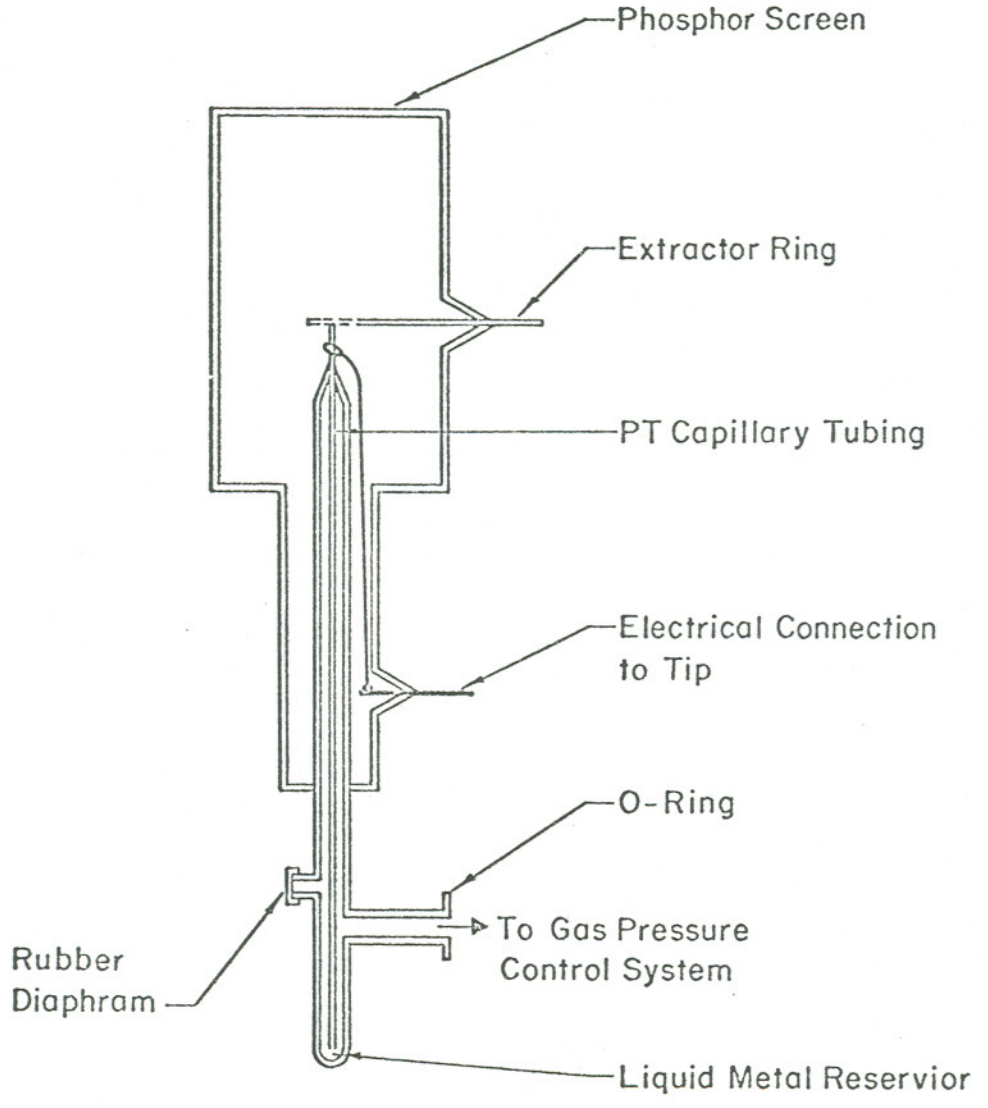

Figure 6. Diagram of first emission chamber and liquid Ga source to provide stable emission.

Ga, since it would now wet the tip rather than shoot off the tip and hit the screen, and (2) allowed high voltages (up to 20 kV) to be used with electrostatic forces unable to pull the liquid Ga off of the needle. Some emission was obtained from this apparatus, however, the leak in Pt-glass seal made control very cumbersome and difficult. Therefore, the apparatus was redesigned as shown in Figure 6.

The longer Pt tube accomplished two objectives. First it allows a longer Pt-glass seal (2 cm) which can be made leak proof. Second, by mounting the apparatus vertically, greater flow impedance is obtained in two ways: (1) the downward force of gravity on a 12 cm high column of liquid metal and (2) the additional length of the Pt tube. The effect of increased flow impedance is to make the flow rate less sensitive to changes in the pressure difference. Therefore, the ability to control the liquid metal is increased.

The addition of the rubber diaphragm allows the vessel to be evacuated before inserting the liquid metal through a hyperdermic syringe, thus preventing any oxidation of the liquid metal.

The liquid metal being used was changed from pure Ga to a Ga/In alloy, containing an eutectic mixture of 12% Wt. In. The change was made because of its slightly higher wetting coefficient, and low melting point (18°C), thus eliminating any need for heating during the experiment.

The experimental procedure for the tubes employing the rubber

diaphragm was to pump the system down to $\approx 10^{-7}$ torr, insert the liquid metal, force it through the needle, check for emission, argon sputter clean the tip, re-establish the vacuum, force the liquid metal through the nozzle, and then check again for emission. This procedure showed sputtering not only helped the liquid metal in wetting the tip, but was necessary to get stable emission. Stable emission was obtained with this apparatus.

The only problem this apparatus presented was an occasional difficulty in forcing the liquid metal through the Pt tube. This difficulty persisted even with extensive pre-use cleaning of the Pt tubing. The problem was eventually found to be caused by the rapid attack by the liquid Ga on the Pt tubing. This is confirmed by the data displayed in Table IV which shows the resistance of Pt to attack by liquid Ga to be very poor.

Based on the information in Table IV, the long Pt tubing was replaced with W and pyrex capillary tubing as shown in Figure 7. W was chosen not only because of its ability to resist attack by liquid Ga, but also its high surface tension. To aid the liquid metal in wetting the needle it is desirable for the needle to have as high a surface tension as possible. This is easily seen from the expression for the wetting angle of a liquid on a solid which is given by:

$$\cos\theta = \frac{\gamma_{SG} - \gamma_{SL}}{\gamma_{LG}}$$

TABLE IV

RESISTANCE OF MATERIALS TO ATTACK BY GALLIUM [8]

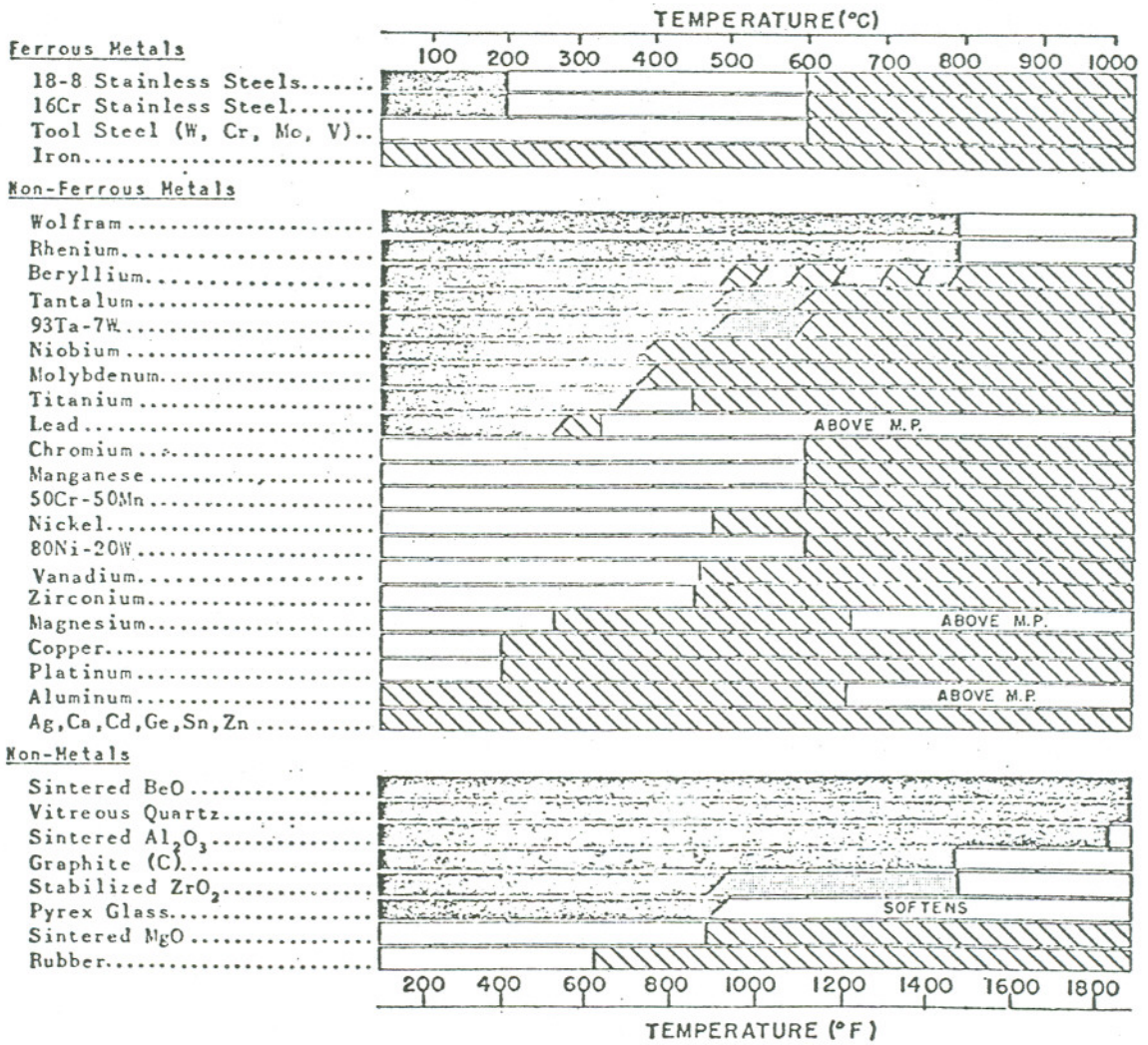

GOOD - consider for long-time use
LIMITED - for short-time use only
POOR - no structural possibilities
UNKNOWN - no data for these temperatures

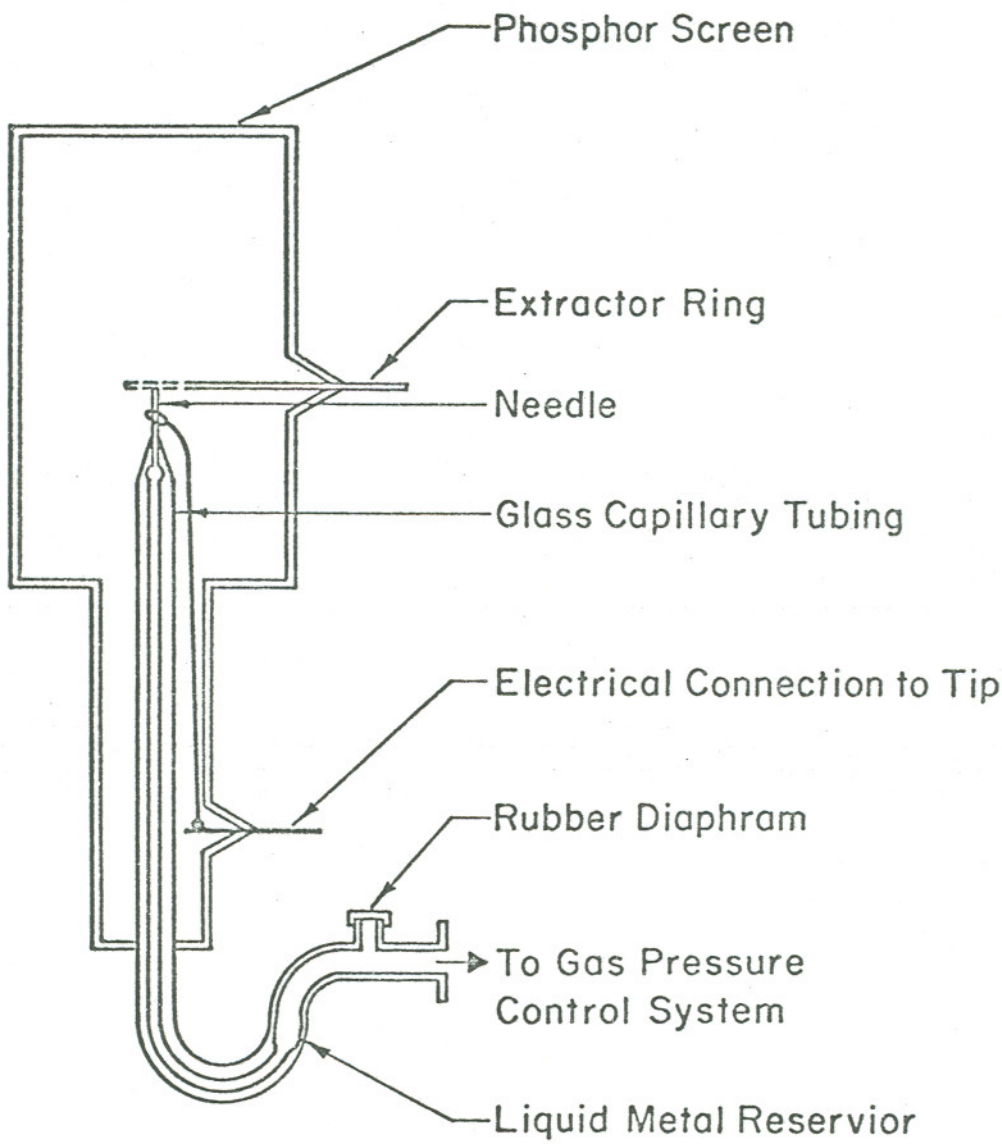

Figure 7. Diagram of emission chamber and liquid Ga source using high Ga resistant materials.

where γ_{SG}, γ_{SL}, γ_{LG} are the interfacial tensions at the liquid-gas, solid-gas, and solid-liquid interfaces respectively. Table V which lists some metals and their surface tensions, shows W to be a good material in this respect because of the higher value of γ_{SG}.

TABLE V

Surface Tension of Selected Solids[9,10]

Material	γ (dynes/cm)	T °C
Ag	1140	907
Al	1140	180
Cu	1670	1047
Fe	2150	1400
Mo	2200	1427
Ni	1850	1250
Pt	2340	1311
Ta	2680	1500
Ti	1700	1600
W	2900	1750
Zn	830	380

The apparatus of Figure 7 provided most of the emission data. The basic design of this apparatus was used to construct a larger more convenient apparatus as shown in Figure 8. Its advantages are a

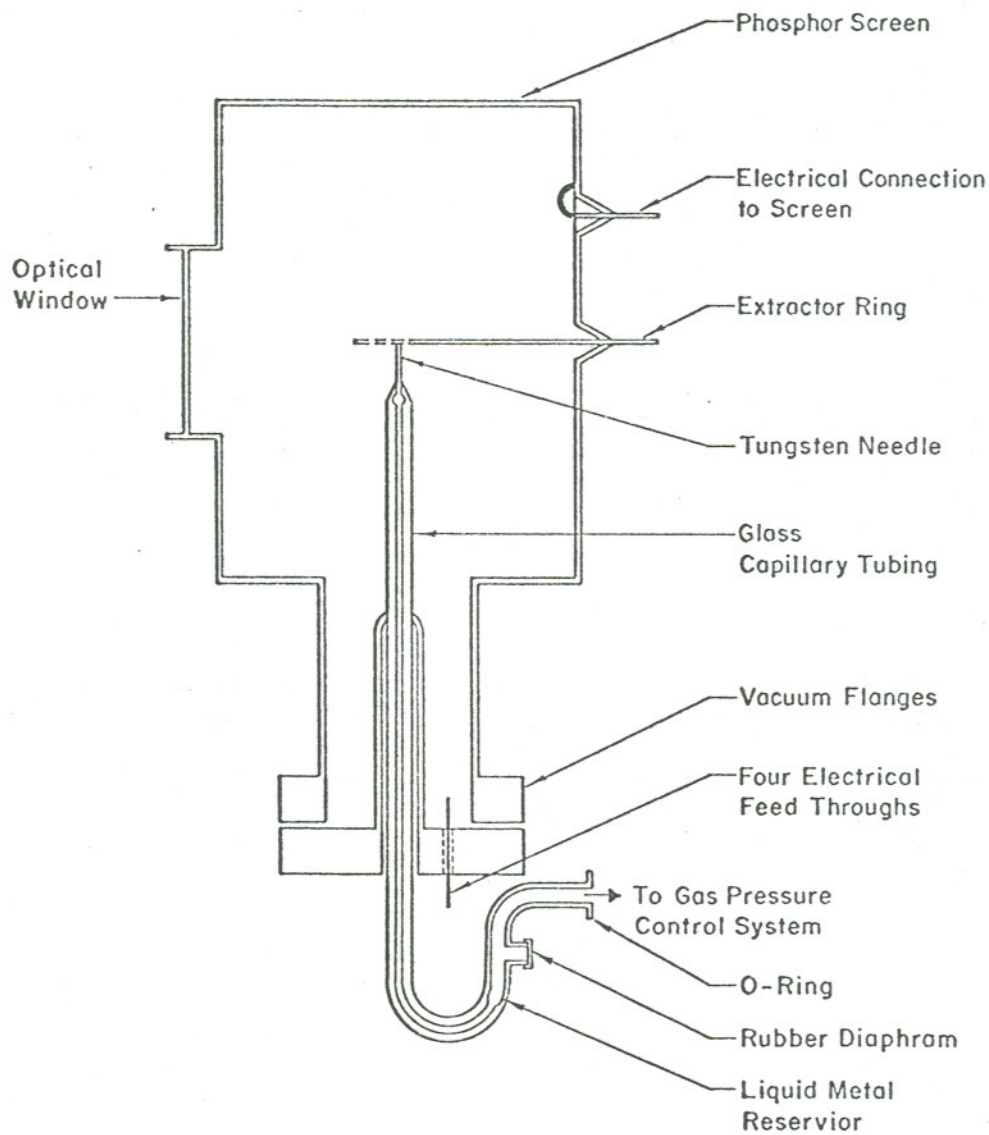

Figure 8. Diagram of the final and most convenient emission chamber and liquid Ga source used.

larger screen to view the emission pattern, an optical window to allow better vision and photography of the nozzle, and flanges to allow assembly and disassembly without glass blowing.

The nozzle configurations that were used are shown in Figure 9. The tips are so shaped to aid the liquid metal in wetting the nozzle. The majority of the emission data was obtained with W nozzles shown in Figures 9(b), (c), and (d).

The nozzle in Figure 9(c) was designed to support a Taylor's cone of half angle 49.3 degrees and base width equal to the inside diameter of the tungsten tube. The emitter insert design of 9(d) supplies liquid metal to the tip end of the emitter through a surface film of Ga wetting the emitter. A small field stabilized cone appears to form on the end of the emitter thus localizing and stabilizing the geometric location of the virtual source. Photographs of both designs actually used are shown in Figures 10 and 11.

Figure 12 shows the simple circuits employed to measure the field emission. The circuit of Figure 12(a) was used to measure the pulse mode of both electron and ion field emission. The attenuator reduced the signal to a magnitude the scope could measure. In measuring the electron emission pulse mode it was found important to match the impedance (50Ω) through the circuit and to reduce induction to a minimum. Also, due to the short duration of the pulse (10 nanoseconds) it was necessary that the scope have a risetime of less than 2-3 nanoseconds, and preferably even faster. The circuit of 12(b) used an R-C

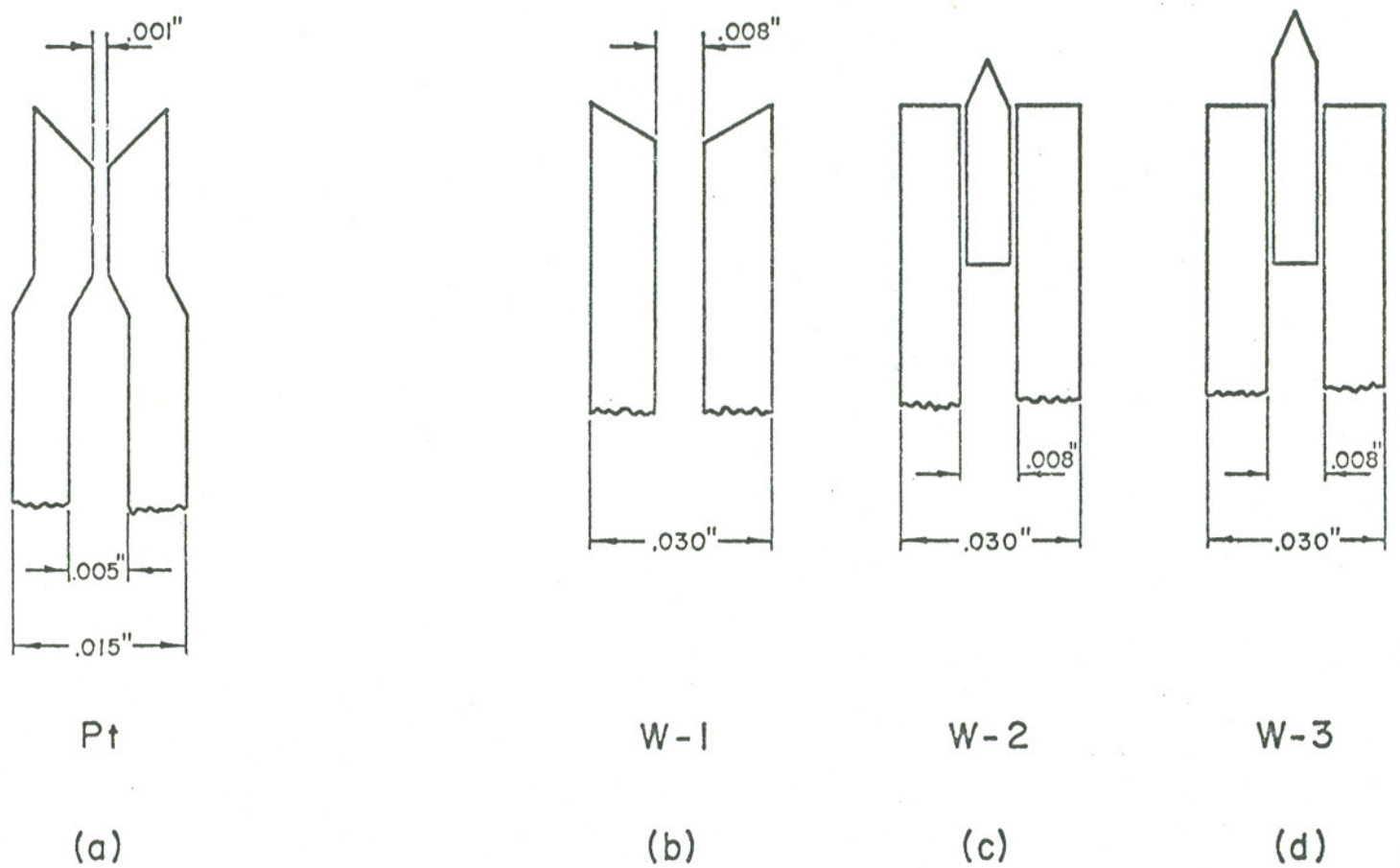

Figure 9. Diagram of the platinum (a) and tungsten (b), (c) and (d) nozzle configurations.

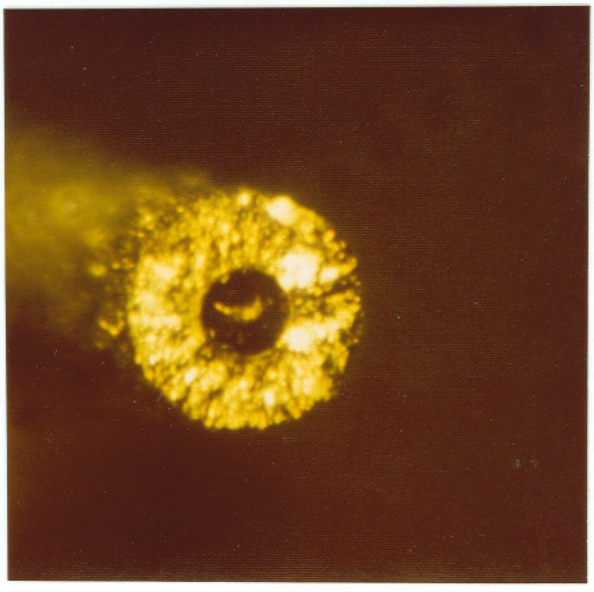

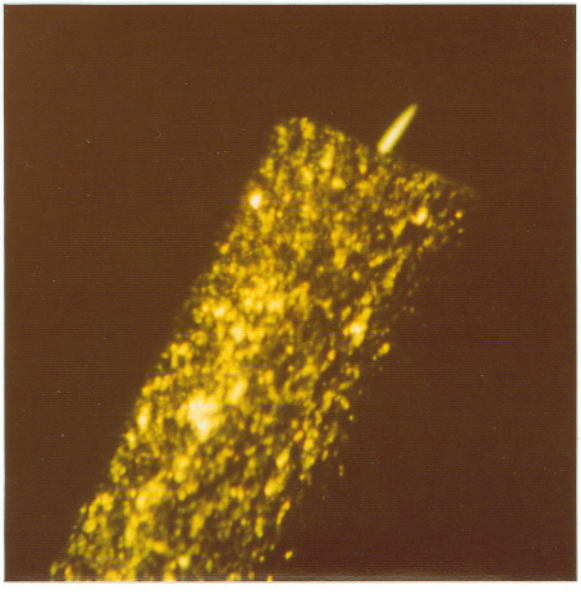

Fig. 10. Top and side view photographs of W-2 nozzle configuration.

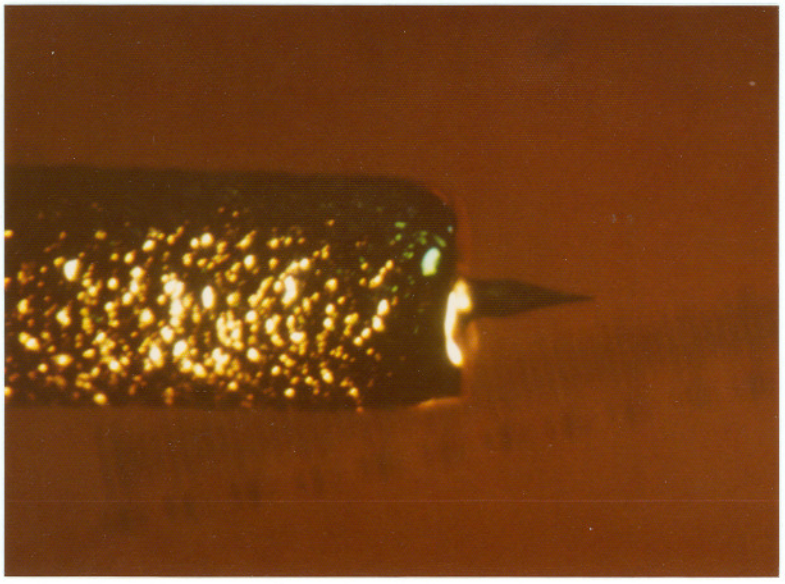

Fig. 11. Photograph of W-3 nozzle configuration.

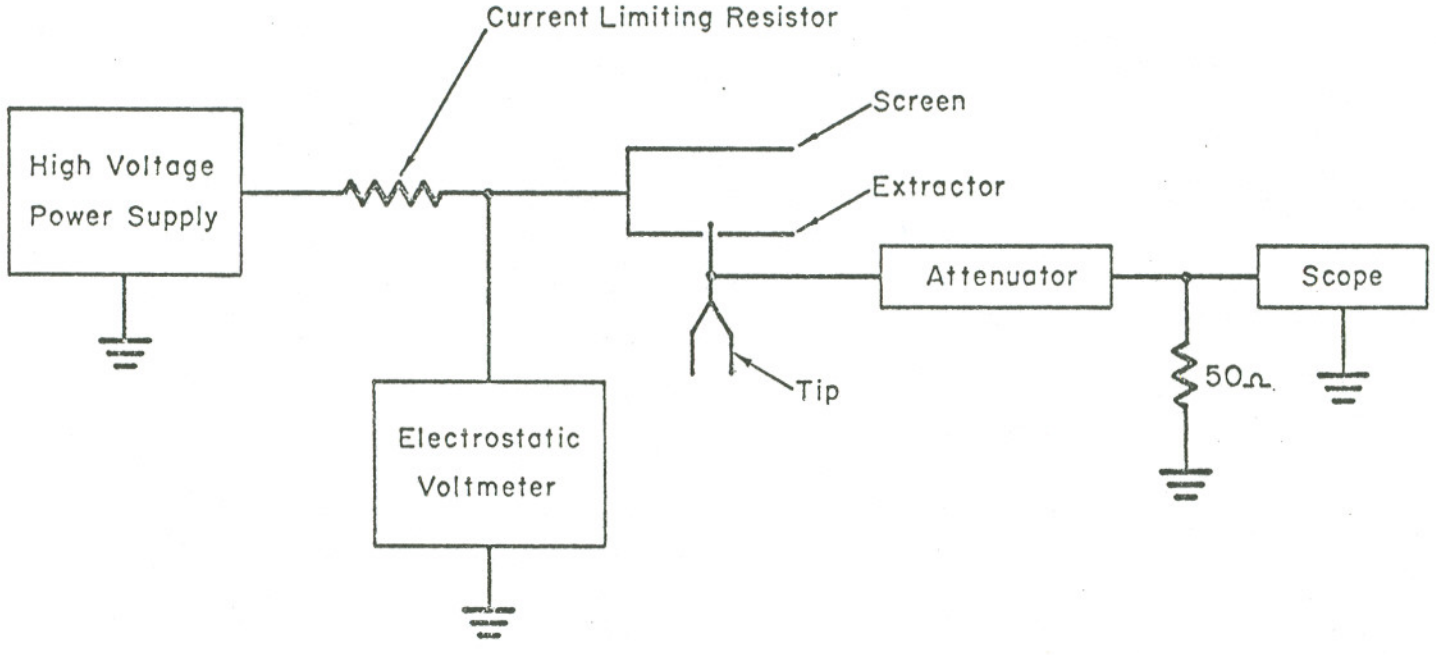

Figure 12a. Circuit used to measure pulse mode of electron and ion emission.

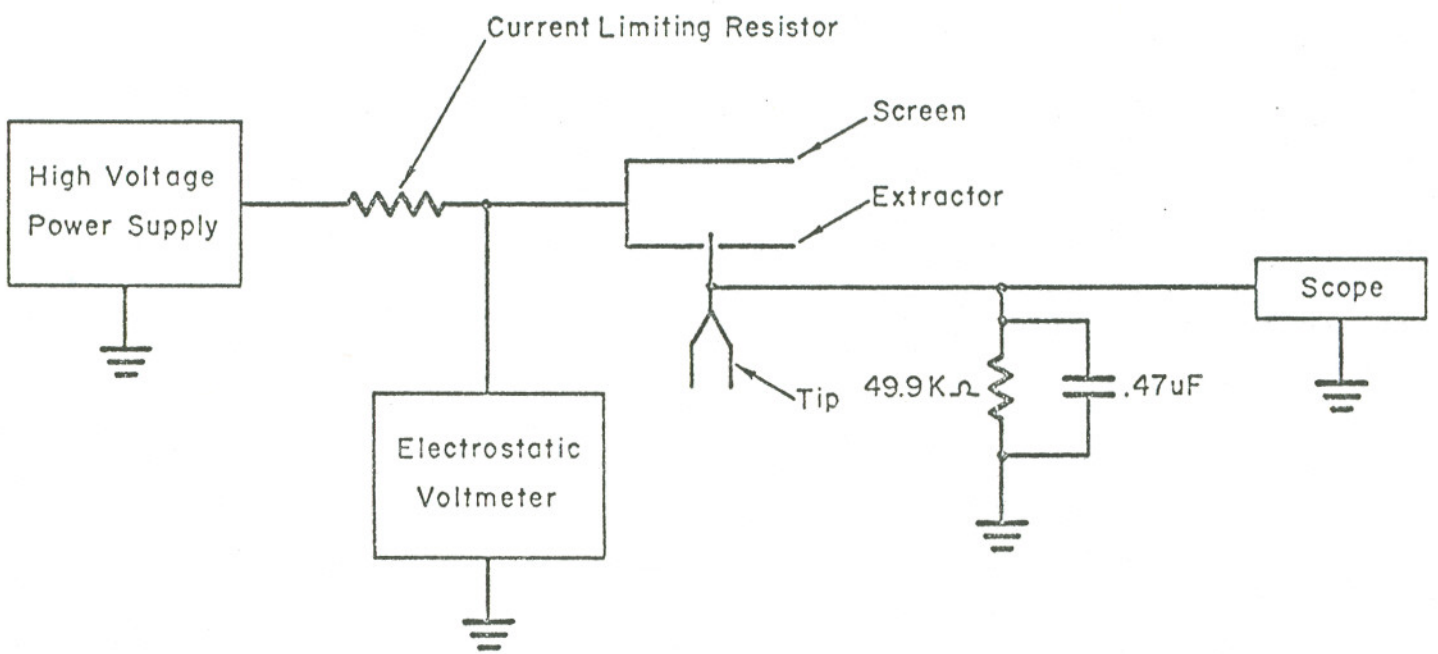

Figure 12b. Circuit used to measure average current during pulse mode of operation.

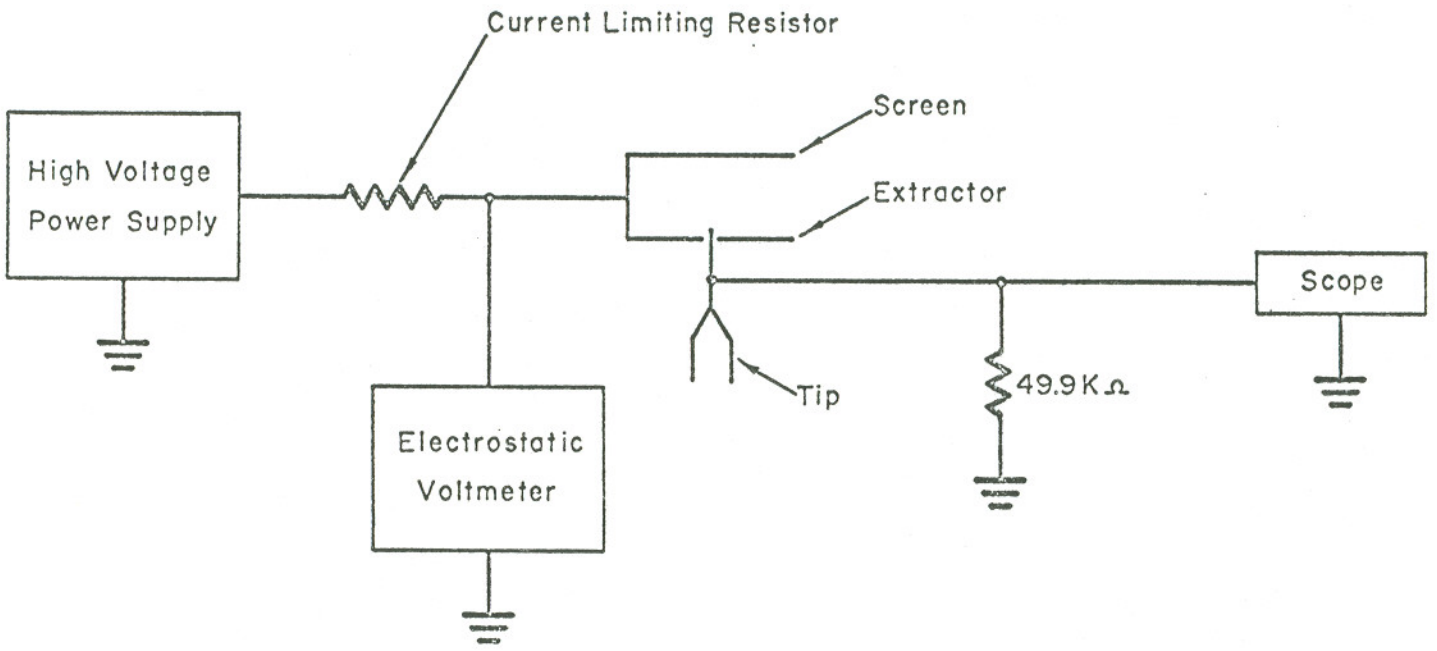

Figure 12c. Circuit employed to measure D.C. ion current.

circuit to enable the measurement of an average current during the pulse mode field emission and 12(c) was used to measure the D.C. mode emission. For life testing the same basic circuit was used with the tip connected directly to a current measuring chart recorder. All components of these circuits were periodically calibrated using a Data Precision Digital Multimeter, which is accurate to 4.5 significant figures.

As previously mentioned, argon sputtering, or in essence a very clean surface, is essential for the liquid metal to wet the surface sufficiently to obtain stable emission. Argon sputtering, which demonstrated itself to be more than adequate in this respect, is somewhat inconvenient; in that an argon source and leak valves must be attached to the vacuum system, exposure of ion pumps to argon can lead to the undesirable condition of argon instability and additional pumping must be done. Therefore, a more convenient technique to clean the tip was devised.

This technique is to resistively heat the inserted W tip of Figure 9(d) to 2000 C; as measured using a pyrometer, in vacuum of $\approx 10^{-6}$ torr. After the tip has cooled, it is removed from the vacuum and immediately immersed in a reservoir of liquid metal. The liquid metal coated tip is next inserted into the W nozzle and the apparatus assembled on the vacuum system and pumped down. The protective coating of Ga prevents the W emitter from becoming oxidized by the surrounding atmosphere. This technique was used successfully to obtain liquid metal emission without argon sputtering.

EXPERIMENTAL RESULTS

Certain liquid metal emission phenomena were exhibited in both the electron and ion modes of emission. Emission was initiated by advancing the liquid metal to the nozzle's end and applying the high voltage. The voltage at which emission usually began was dependent on the nozzle configuration. Table VI lists the threshold voltages for the various nozzle configurations. The difference in the threshold voltage of W-2 and W-3 needles can probably be attributed to the difference in the length of the inserted emitter.

TABLE VI

Threshold Voltages for Each Nozzle Configuration

Nozzle Configuration	Threshold Voltage (kV)
Pt	8.5 - 9.0
W-1	9.8 - 10.5
W-2	12.0 - 12.5
W-3	7.5 - 8.5

To obtain stable emission it was critical to have the "proper" amount of liquid metal on the nozzle's end. More, or less, than the proper amount results in an unstable form of emission. For the configurations of Pt and W-1, the proper amount of liquid metal was that which would result in the liquid metal forming an upright cone

approaching Taylor's theoretical half angle of 49.3°. Figure 13 shows a photograph of the nozzle and liquid metal cone formed during electron emission. When the cone formed, emission was very stable throughout the voltage range (9 to 20 kV). If too little liquid metal was at the nozzle, then emission occurred from a small cone formed on (Figure 14) the edge of the nozzle. The cone provided a steady current if the voltage remained constant, but moved spatially and often formed multiple emission points as the voltage was increased. Excess liquid metal on the nozzle caused an unstable upright cone to form that was in continuous motion and provided very unstable emission.

The nozzle configuration of W-2, which has an inserted tip specifically designed to support a Taylor's cone, had several amounts of liquid metal which could be considered proper. The first was that amount which does form a stable Taylor's cone over the inserted tip. This Taylor's cone was slightly, but not significantly more stable than the Taylor's cone obtained with the Pt and W-1 nozzles. Similar to the previous nozzle configuration, excess liquid metal on the tip provided unstable emission from an unstable upright cone that was in continuous motion. Quite often these unstable cones would form elongated tips which at a constant voltage would sometimes become stable (Figure 15), thus demonstrating experimentally that a truncated cone and cylinder geometry can be a stable geometry.

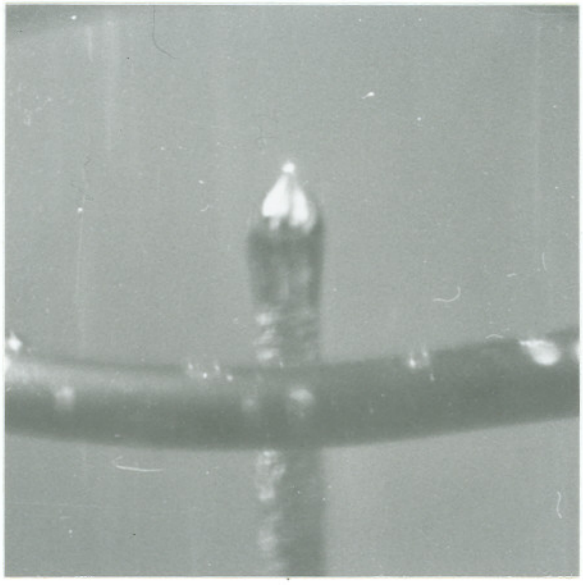

Fig. 13. Photograph of unsupported liquid Ga cone formed on W-1 nozzle.

Less liquid metal than necessary to form a Taylor's cone would result as in Figure 16 with emission coming from the point of the inserted tip. This emission from a small localized cone on the end of the inserted tip produced stabler emission characteristics than the Taylor's cone. A little less liquid metal would result in a small cone forming as shown in Figure 17. At a constant voltage, this cone would provide steady emission, but moved spatially and caused unstable emission as voltage was changed. Often in this circumstance, emission came from both the inserted tip and the small cone simultaneously. Slightly less liquid metal on the nozzle end would prevent the small cone from forming and only a very stable emission from the point of the inserted tip would occur. The stability of emission from this type of situation was the reason for the designing of the W-3 configuration with the longer emitter.

The W-3 configuration was designed for emission from the point of the inserted emitter by liquid metal supplied via self-diffusion along the emitter shank. Therefore, the proper amount of liquid metal would be a small amount about the base of the shank as in Figure 18. This was the case experimentally as is easily seen in Figure 19, which are photographs of the nozzle with and without emission. The only emission instability came from an excess amount of liquid metal causing very large unstable cones to form. However, by applying voltages of 18-20 kV this excess liquid metal could be, by the electrostatic forces, pulled off of the nozzle, leaving a proper

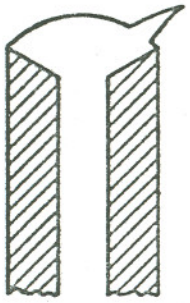

Figure 14. Cone forming with too little Ga on Pt- or W-1 tip.

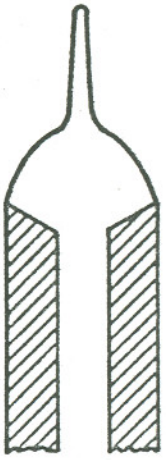

Figure 15. A stable . geometry of a truncated cone and cylinder formed with excess Ga on nozzle.

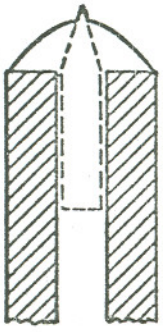

Figure 16. Proper amount Ga on W-2 nozzle to result in stable emission from point of inserted emitter.

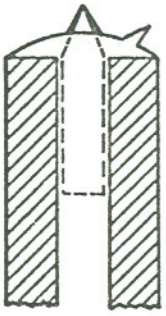

Figure 17. Emission from small cone and point of inserted emitter simultaneously.

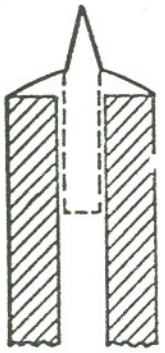

Figure 18. Proper amount of Ga to obtain stable emission from W-3 nozzle.

(a)

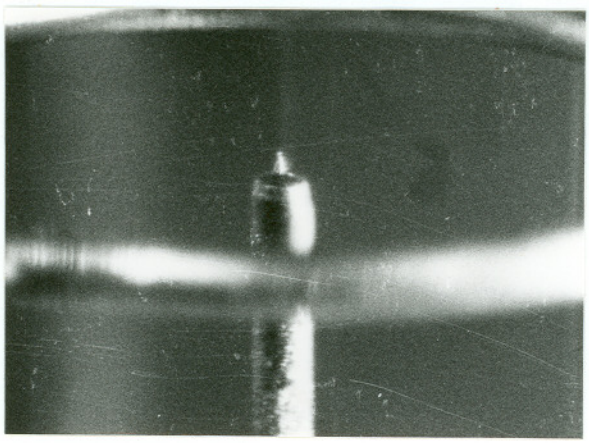

(b)

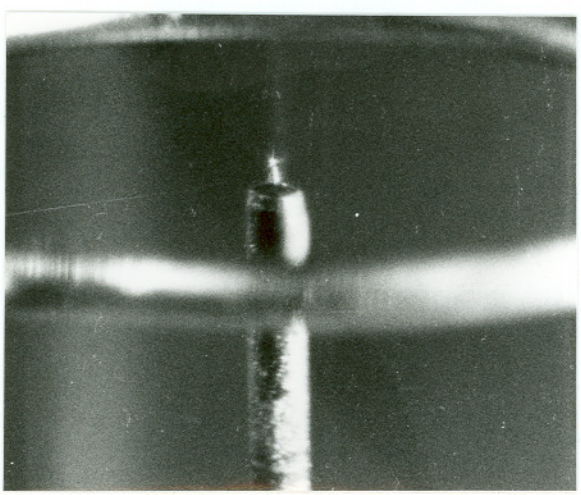

Fig. 19. Photographs of W-3 nozzle while not emitting (a) and during electron emission (b).

amount of liquid metal behind for stable emission from the point of the inserted tip. This nozzle configuration produced the greatest degree of emission stability.

Once the proper amount of liquid metal was on the end of any of the nozzle configurations, then the emission became very stable and the emission characteristics consistent. The threshold emission voltage remained constant, and the emitting cone could be made to collapse and re-form repeatedly by varying the voltage across the threshold voltage. The emission characteristics are very constant over a period of time, as it was possible to leave the system off over a weekend and measure the same characteristics. For a given cone, the threshold voltage was very sharply defined, ± .1 kV. The voltage at which emission ceases and the threshold voltage were identical. An apparent exception to this was the W-3 nozzle configuration, because sometimes the apparent threshold voltage was higher than the ceasing voltage. In these cases, a higher voltage than the normal threshold voltage was required to wet the point of the emitter with liquid metal. But, once the point of the inserted emitter was supplied with metal, the threshold and ceasing voltages became equal.

The ability of the liquid metal to wet the nozzle was an important factor in obtaining and maintaining emission. Without cleaning the nozzle, either by argon sputtering or the heating technique, the liquid metal would not wet the nozzle sufficiently to permit emission. Instead, the electrostatic forces would pull

the liquid metal off the end of the nozzle at voltages lower than the threshold voltage.

With the W-3 nozzle, the wetting ability of the liquid metal has even greater importance as it is directly related to the ability of the liquid metal to self-diffuse to the emitter's tip. The importance of wetting ability in supplying liquid metal to the emitter tip was demonstrated during a series of life tests. The first life tests ended in less than an hour when the supply of liquid metal at the emitter tip was exhausted. The nozzle was cleaned by argon sputtered, thereby increasing the wetting ability of the liquid metal. The following life test lasted 25 hours, the second 16 hours. These life tests ended when the liquid metal supply at the base of the emitter was exhausted. Thus, to obtain and maintain emission the liquid metal must wet the nozzle surface, and this necessitates argon sputtering or heat cleaning of the nozzle.

Perhaps the most distinctive feature of Ga field emission is a small spot of incandescent light surrounded by a blue glow at the emitting site. The intensity of both the incandescent and blue glow increases with increasing current and enables one to discern precisely the location of the emitting site.

The before and after emission experiment photographs, as seen in Fig. 20, of the W-2 and W-3 nozzles, reveal that the inserted emitter becomes dulled and rounded off. This was most likely due to the argon sputtering.

(a)

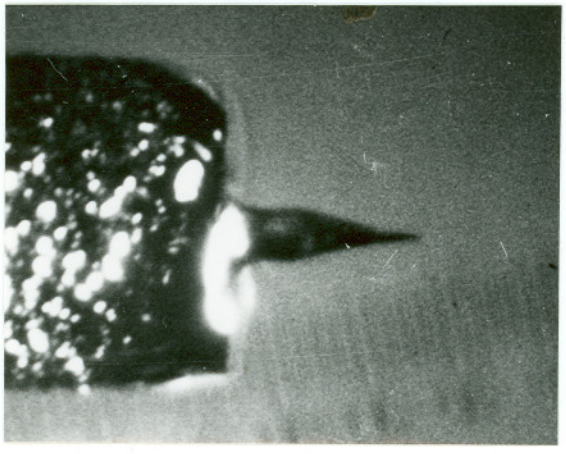

(b)

Fig. 20. Photograph of W-3 nozzle before emission experiment (a) and after emission experiment (b).

I. Electron Emission

Electron emission has exhibited only one mode of operation, the pulse mode. This mode is characterized by high current, and short duration pulses which occur at a constant rate producing average current of 1 μA to 6.5 mA.

The general emission characteristics were the same for all of the nozzle configurations. Each configuration produced stable emission throughout the voltage range. However, the nozzle configurations with the emitting cone formed on the inserted emitter were more stable than the configurations designed for formation of an unsupported Taylor's cone, especially at the higher voltages (16 kV). Occasionally at the higher voltages (16-20 kV), the Taylor cone would break down by forming multi-emission sites. This was accompanied by an immediate sharp increase in the average current. A typical case is shown in Fig. 21. Emission from the end of the inserted emitters demonstrated no tendency to degenerate into an unstable mode.

A typical pulse produced by the W-1 and W-2 nozzle, as shown in Fig. 22(a) was 90-120 A, approximately 10 nanoseconds in duration, risetime of 3-4 nanoseconds, and Gaussian in shape. A similar pulse (Fig. 22(b)) of 40-60 A was obtained from the W-3 nozzle. The pulse maintained its general shape and was of constant duration for any combination of load resistor and voltage, while its magnitude increased slightly with a large increase in current. The pulse rate

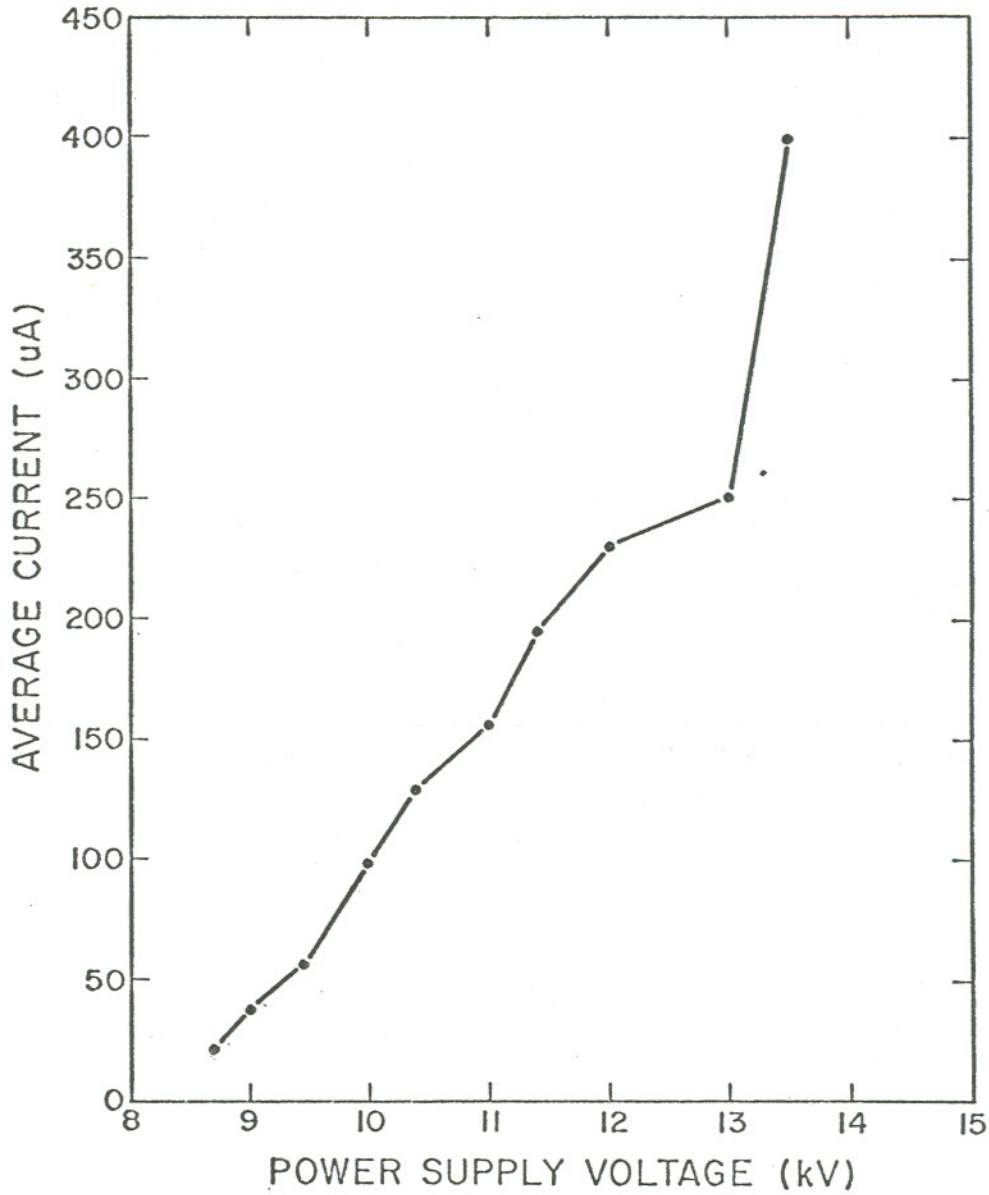

Figure 21. Sharp increase in average current caused by the formation of multi-emission sites.

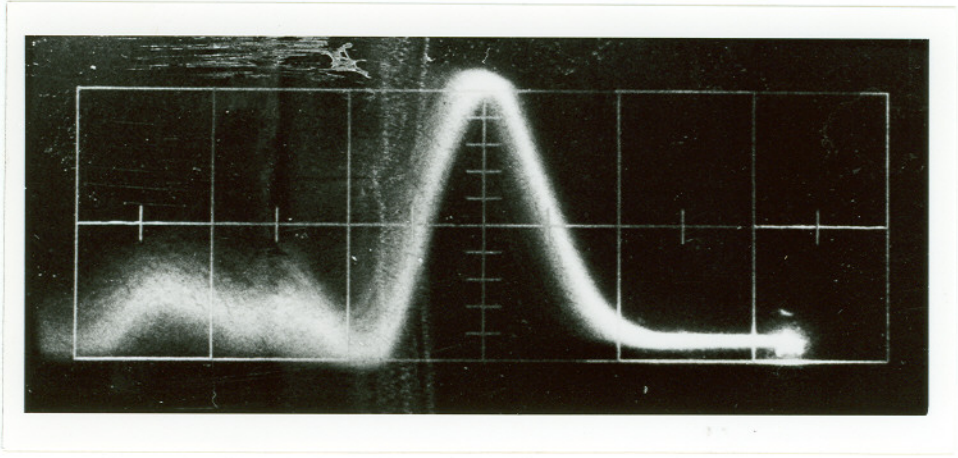

(a) 50 Amps/div and 5×10^{-9} sec/div

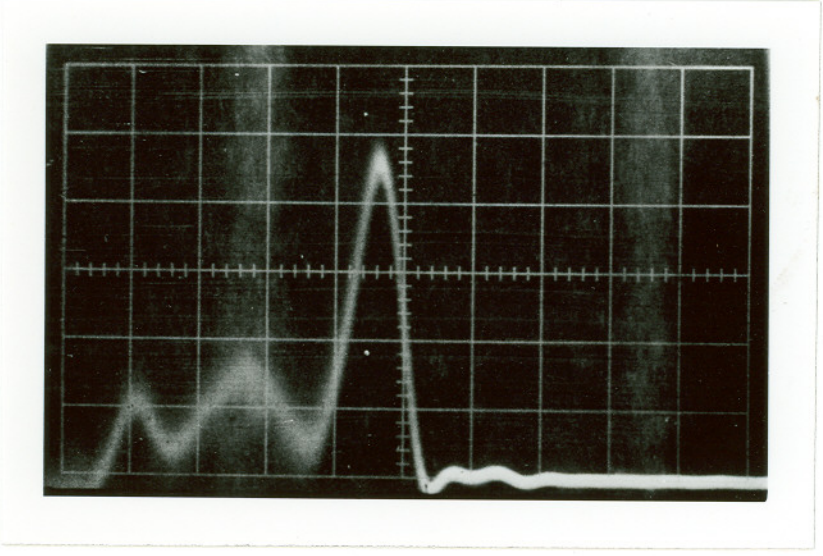

(b) 10 Amps/div and 5×10^{-9} sec/div

Fig. 22. A typical electron pulse from Pt. W-1, W-2 nozzles (a) and from W-3 nozzle (b).

increased with increasing voltage and decreasing current limiting resistor value, as shown in Figures 23 and 24. Since the total current per pulse was essentially constant, the change in average current was due to change in the pulse rate and not the pulse shape. The measured pulse frequency varied from 40 pulses per second to 5500 pulses per second corresponding to average currents of 4 μA and 460 μA respectively. A maximum pulse frequency of 8×10^4 pulses per second can be calculated, based on the maximum measured average current of 6.5 mA.

Figure 25 shows the voltage traced at the anode electrode of the tube. The sharp drop in extractor voltage was due to liquid metal discharge shown in Figure 22 which was followed by a charging rate governed by the tube capacitance, voltage, and load resistance.

The voltage at the anode electrode shown in Figure 25 exhibits a pattern similar to an R-C circuit. The period of this pattern and the period of the pulses were shown to be equal by almost simultaneous measurement. This indicates that the tube was acting as a capacitor, storing up charge and then discharging during the pulse. Thus, increasing the voltage or decreasing the current limiting resistances allowed the apparatus to charge more rapidly and thus increase the pulse rate. By considering the system as an R-C circuit with the glass tube as a capacitor, then the time, t, to charge the capacitor is:

$$t = -RC \ln \frac{V - V_o}{V} \tag{28}$$

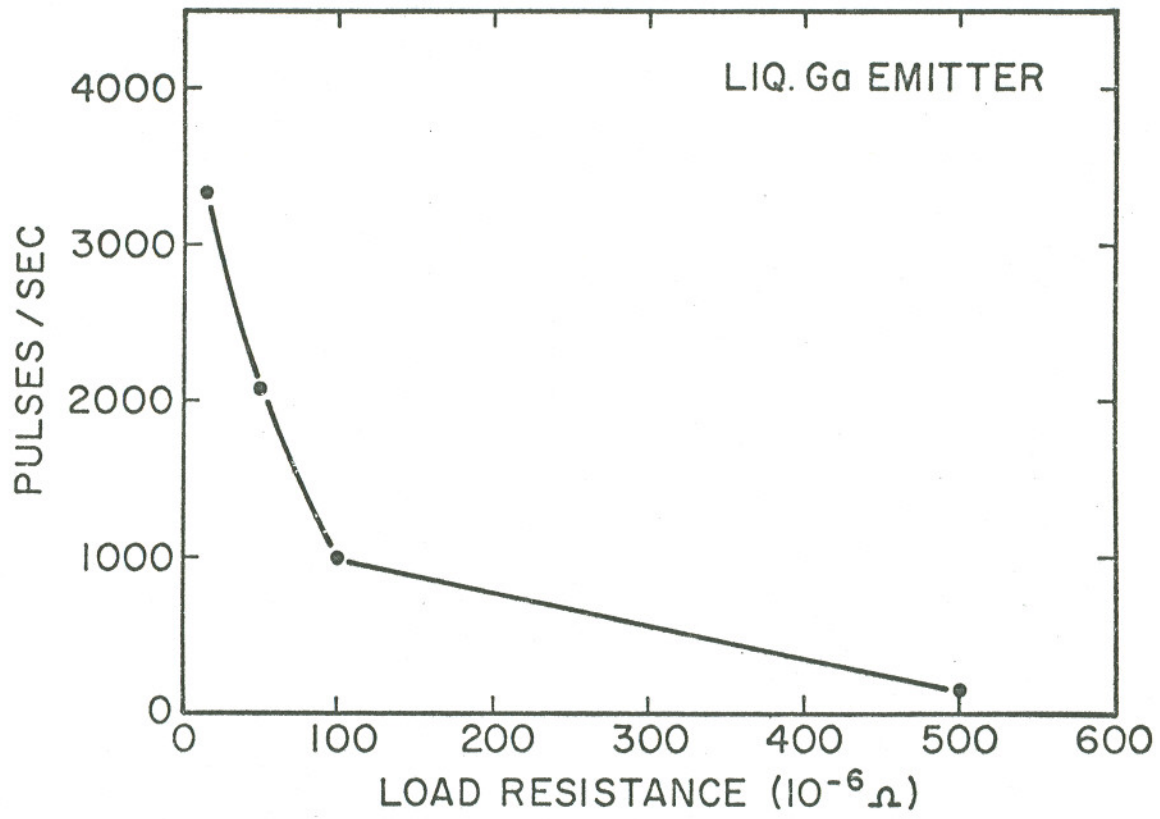

Figure 23. Plot of the pulse rate of electron emission from liquid Ga vs load resistance for a power supply voltage of 12 kV.

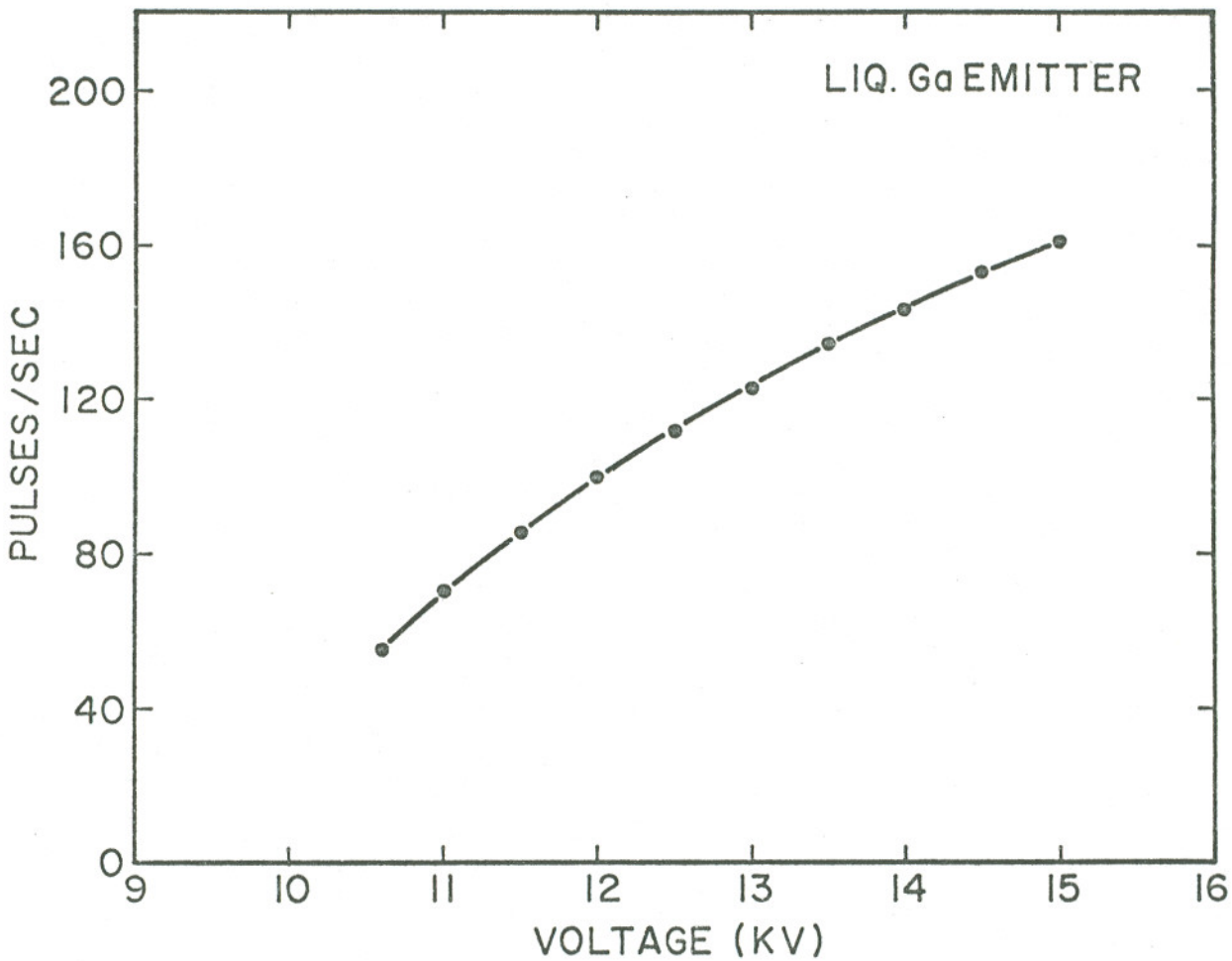

Figure 24. Plot of pulse rate vs power supply voltage for electron emission from liquid Ga using a load resistor of 500 MΩ.

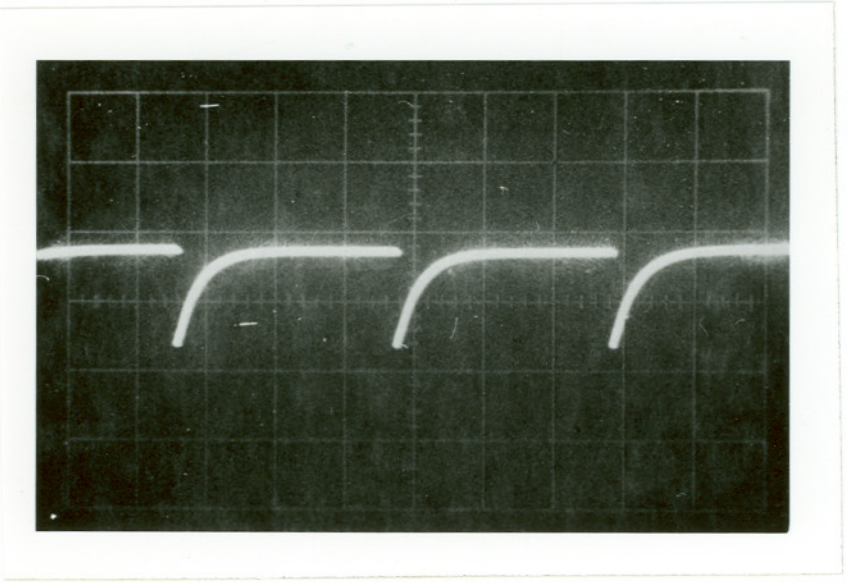

Fig. 25. A photograph of voltage and of trace of RC charge build up on tube and anode. Time base is 1 m sec/div and amplitude is 10 kV/div.

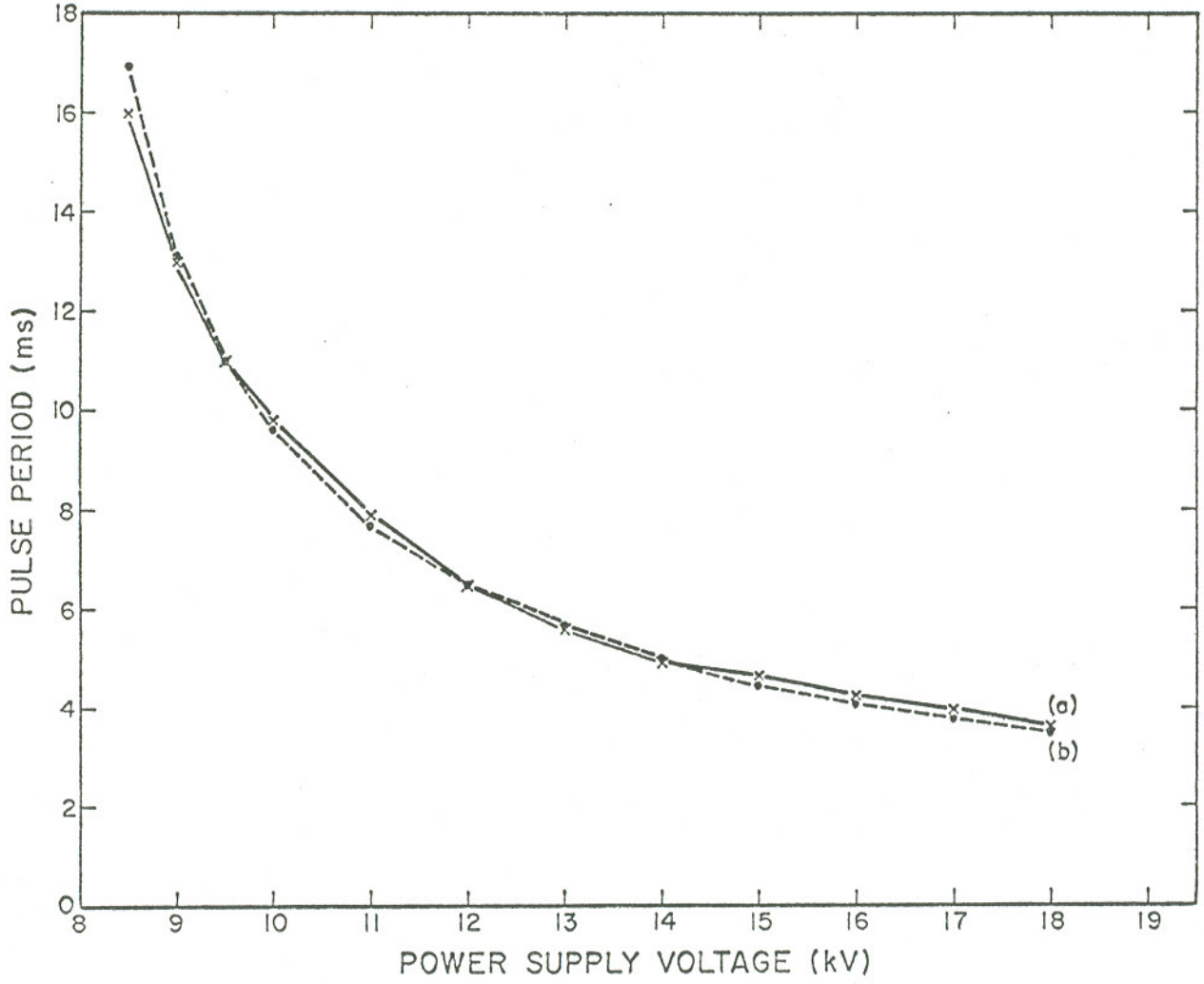

Figure 26. Comparison of the measured electron pulse period (a) and calculated pulse period (b) for a 500 MΩ load resistance.

where R is the load resistor and C is the tube capacitance. The calculated pulse period obtained from the above equation, as shown in Figure 26, is in reasonable agreement with the measured pulse period. A tube capacitance of 12×10^{-9} F was calculated.

The average current increases with pulse frequency which, in turn, increases with increasing voltage or decreasing load resistances. This can be seen in Figure 27 curves which are typical average current data. The direct relationship between average current and pulse frequency becomes evident in the comparison of the average current and pulse frequency data of Figures 27 and 28.

An average current can be calculated based on data providing the current per pulse and pulse frequency. Figure 29 shows this calculated current to be in fairly good agreement with the measured average current, as it should be. These calculations assumed a constant magnitude for the pulse, resulting in 8×10^{-8} C of total charge per pulse.

The maximum average current measured was 6.5 mA at 10.6 kV and without a current limiting resistor. This current was sufficient to heat the extractor electrode to a red glow within several seconds. Therefore, higher pulse frequencies and corresponding higher currents were not investigated, but there is no reason to believe they are not possible.

The results of the life testing are compiled in Table VII. Each life test self-terminated when the supply of liquid metal on

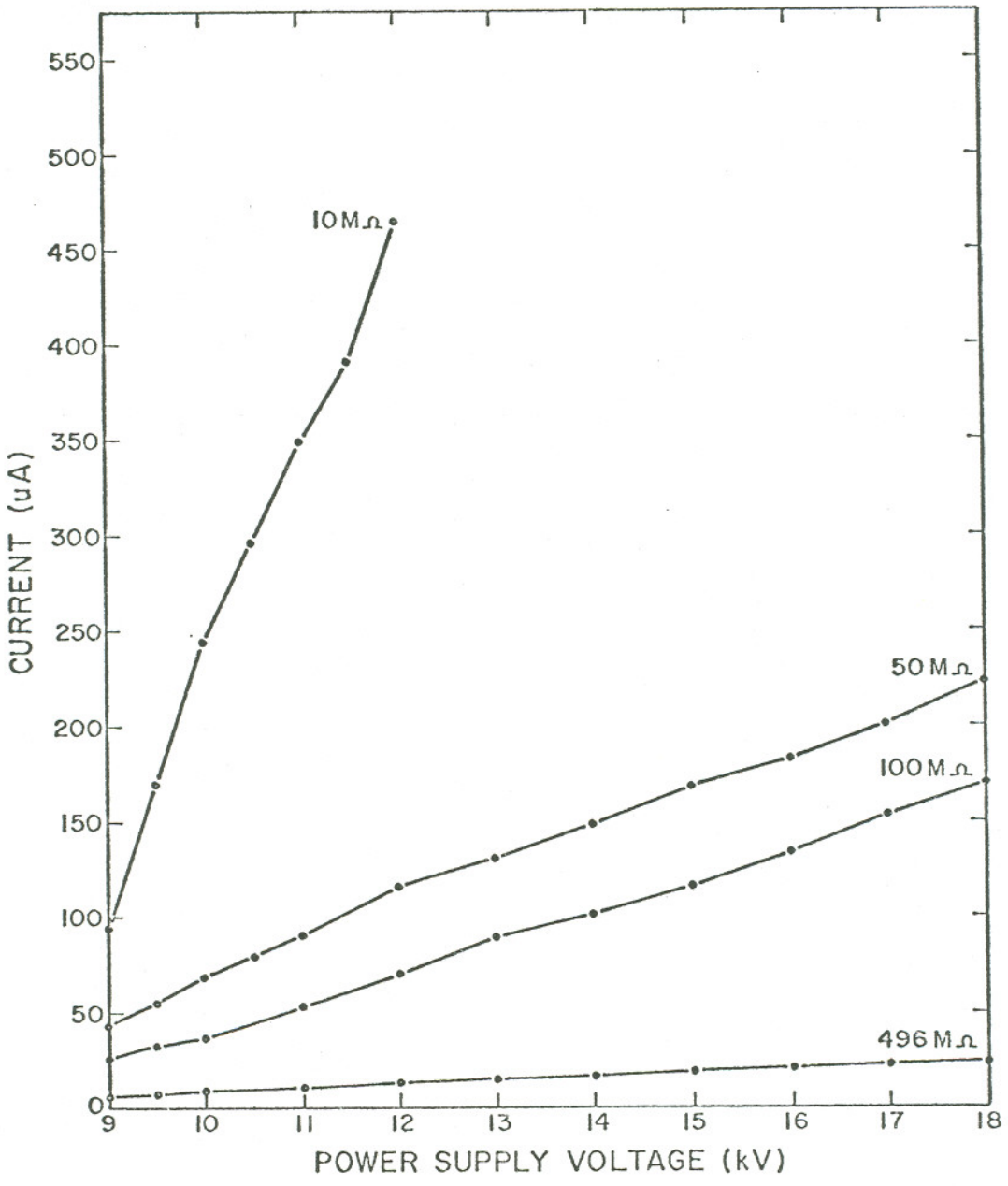

Figure 27. Average electron emission current vs voltage for various load resistances.

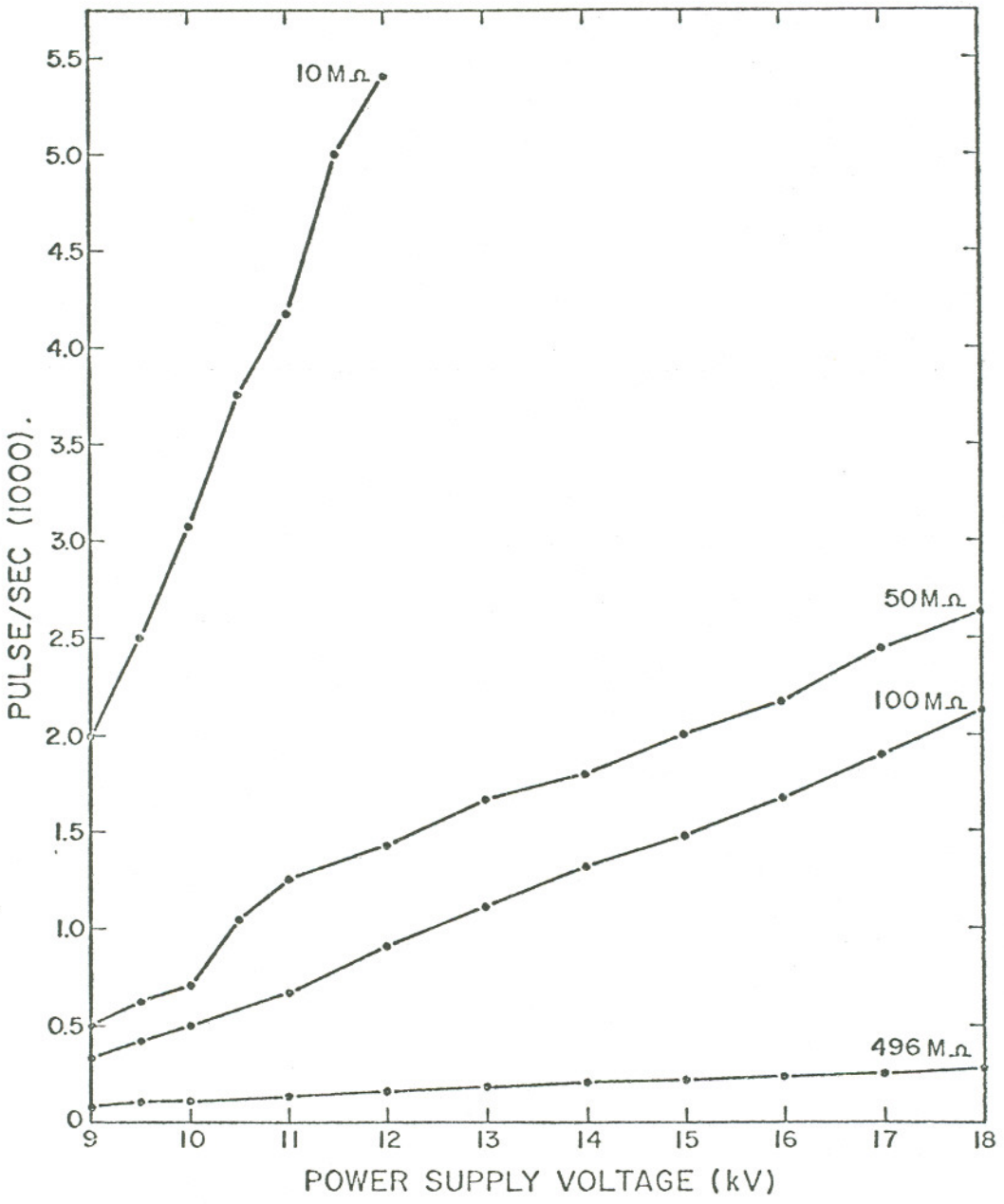

Figure 28. Electron emission pulse frequency vs voltage for various load resistances.

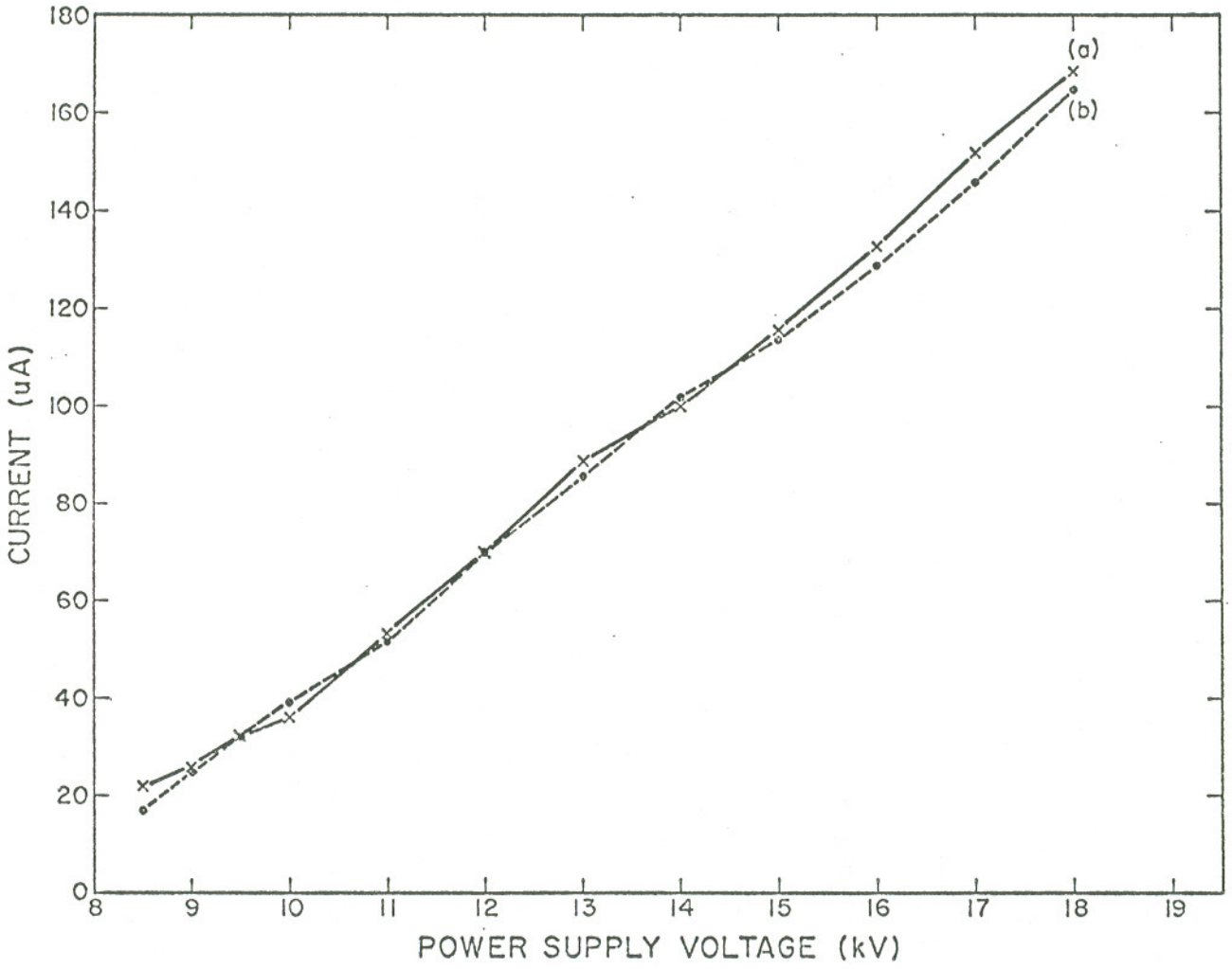

Figure 29. A comparison of measured average current (a) and calculated average current (b) based on pulse magnitude, duration and frequency data.

TABLE VII

Summary of Electron Life Tests

Nozzle	Power Supply Voltage (kV)	Load Resistor (MΩ)	Average Current (μA)	Duration (hrs)
Pt	16.8	661	275	.92
Pt	16.5	66	275	.98
W-3	14.0	100	80	5.5
W-3	12.0	100	100	7.5

the nozzle disappeared. The two reasonable explanations for its disappearance are (1) the liquid metal was used up by the emitting process and (2) the liquid metal flowed back into the nozzle. Since the latter does not occur over a period of many days when the system is not in use, then the first explanation is accepted. This means, that the electron emission process used or emits a definite amount of liquid metal. This is contrary to regular field emission theory where electron emission requires no supply of emitter material.

The life testing indicates that continuous stable emission could be maintained for as long as the proper amount of liquid metal could be supplied to the nozzle.

The emission pattern on the phosphor screen, as shown by the photograph in Figure 30, has no structure and fills the entire screen. Relative intensity measurements made by measuring the relative density of negatives of the photographs taken of the screen

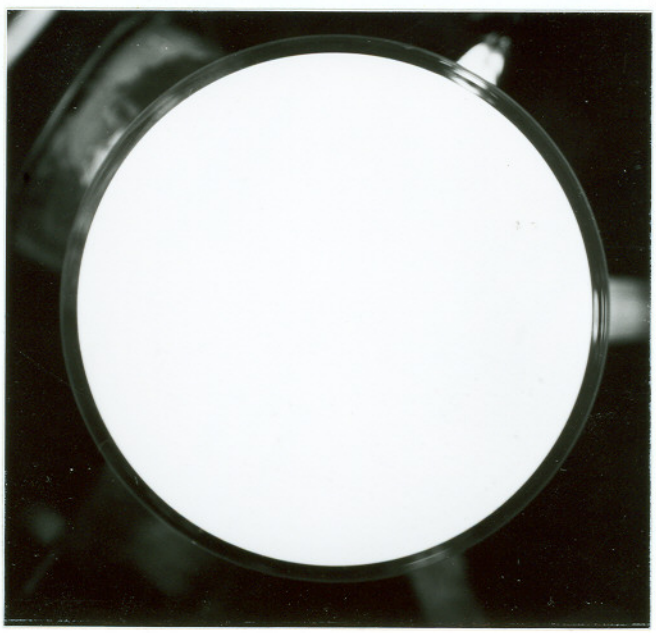

Fig. 30. Photograph of electron emission pattern.

showed essentially a uniform intensity with a slight radial decrease amount to 1 - 3% at the far edges of the screen. The edge of the screen corresponds to an emitting half angle of 40.5°.

II. Ion Emission

Ion emission exhibited three different modes of operation, a D.C. mode, high frequency mode, and a pulse mode. Typical D.C. mode current - voltage characteristics obtained from the W-3 nozzle are shown in Figure 31. As can be seen from Figure 31, the current limiting resistor has a major effect on the I - V curve, however, for all values of the current limiting resistor the I - V curves are closely approximated by a straight line. The current - voltage curves exhibit a slight hysteresis as shown in Figure 32. As in the electron pulse mode, the D.C. mode emission characteristics are less erratic with increasing value of the current limiting resistance. A peak D.C. current of 500 μA was obtained at 16 kV, and 10 MΩ current limiting resistance. This current was maintained only for several seconds, because by then the nozzle was glowing red from the secondary electron bombardment. There was no indication that higher currents could not be obtained.

In the high frequency mode the collected current exhibited a non-uniform high frequency on the order of 100 kHz. This mode always degenerated into the D.C. or pulse mode usually within several seconds and always less than 20 seconds.

The pulse mode has the same characteristics as the electron pulse mode with the following differences: the pulse is smaller, about 2.2 mA, the average currents are smaller, and the pulse rate is

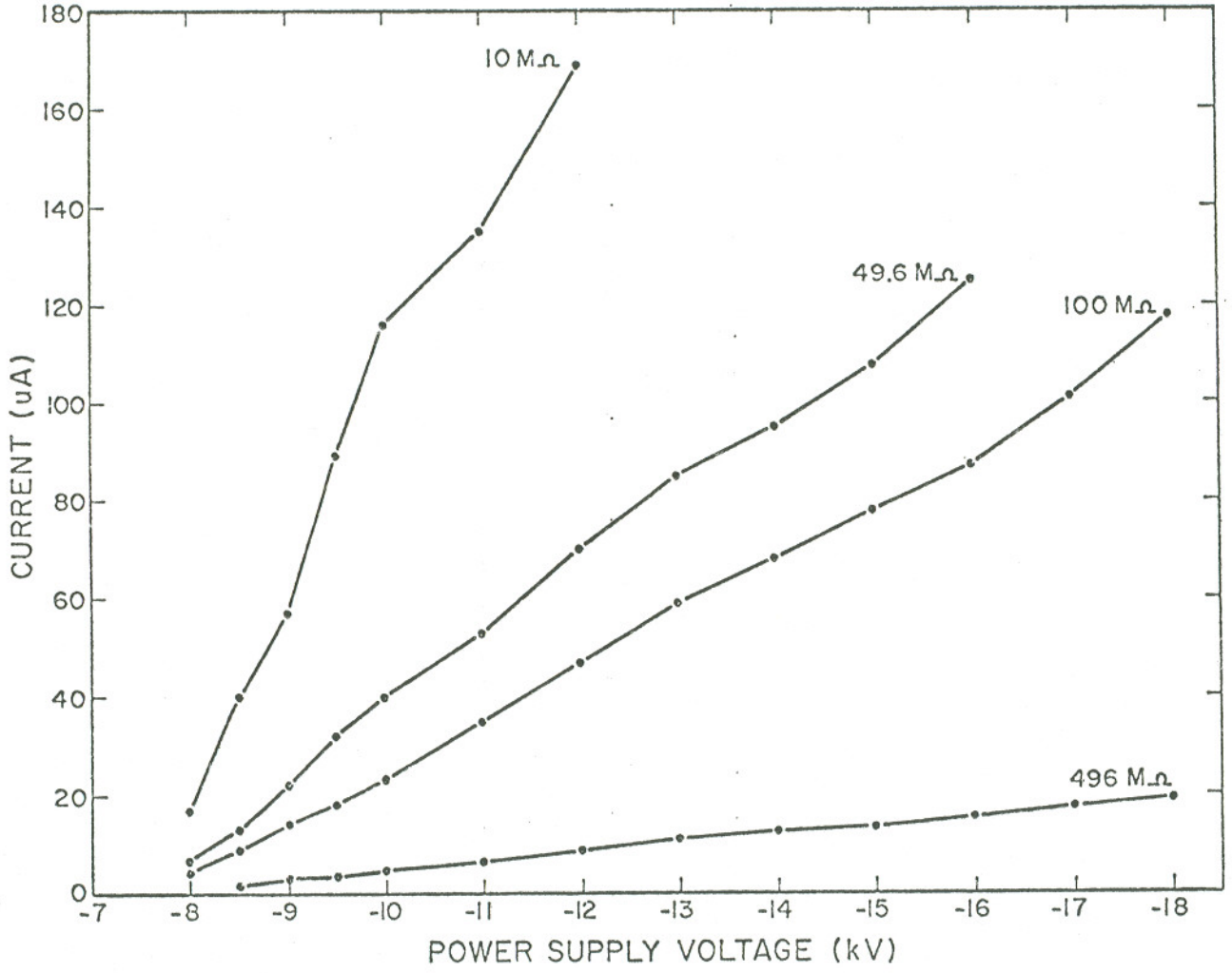

Figure 31. A plot of D.C. ion current vs voltage for several current limiting resistances.

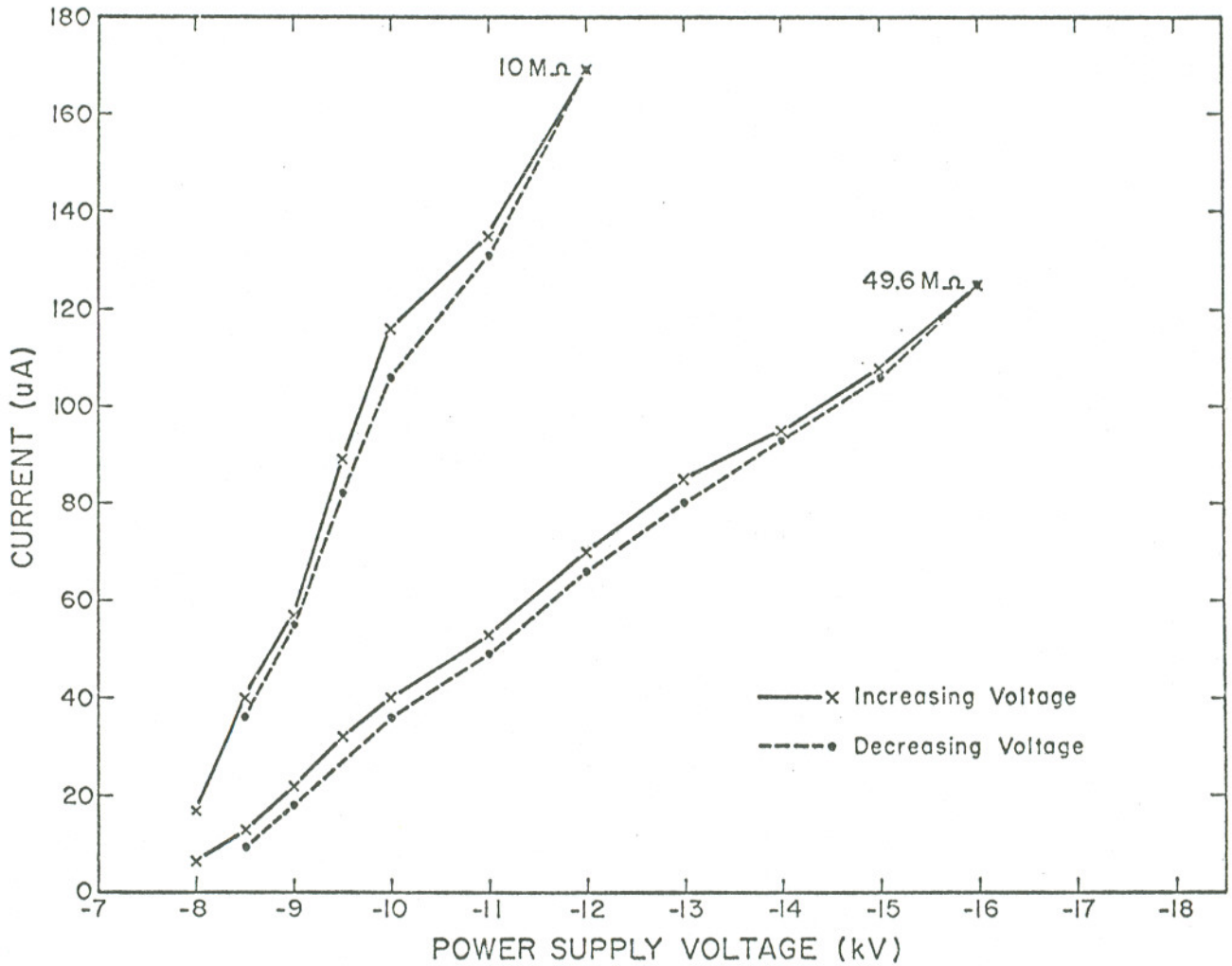

Figure 32. A plot of D.C. ion current vs increasing voltage and decreasing voltage.

slower and only constant to a factor ± 0.1 ms. This slight inconsistency of the rate results in a nonconstant triggering of the scope which prohibits viewing of a single pulse. Average currents of 1 μA to 2.5 mA were obtained in this mode. Again, higher currents were not attempted because of the heating of the needle to a red glow by back scattering electrons. However, the indications are that higher currents are possible.

The nozzle configuration had a major effect in determining which mode of emission was obtained. The configurations in which the emitting site was formed on the end of the inserted emitter produced mostly D.C. mode emission and the configurations on which an unsupported Taylor cone was formed yielded primarily the pulse mode. Only the pulse mode was obtained from the Pt nozzle and the similar W-1 nozzle was mostly pulse mode with very limited amount of D.C. emission. It was obtainable only with a 10 MΩ current limiting resistor in a limited voltage range of 12 - 14 kV and could only be maintained for approximately 60 seconds before it would degenerate into the pulse or high frequency mode.

With the W-2 nozzle, all three modes were easily obtained. Generally as the voltage was increased, the pulse mode was obtained, then the high frequency mode, which would degenerate into either pulse or D.C. mode, and then the D.C. mode.

The D.C. mode was obtained most easily with current limiting resistances of 10 to 100 MΩ. The D.C. emission was quite erratic

and inconsistent from one moment to the next. A frequently seen phenomenon was at a constant voltage the D.C. current would slowly rise from A μA to B μA in about 8 - 10 seconds. At B μA the mode would change from D.C. to the high frequency mode which would degenerate to the D.C. mode at A μA after approximately 5 seconds. This pattern would repeat itself many times. The current at A and B increased with voltage although the difference remained constant. While this pattern was observed in the D.C. mode, by continuously varying the high voltage, a steady D.C. current could be maintained. Therefore, it is expected that a feedback circuit could probably produce a steady D.C. current in this situation.

The W-3 nozzle produced stable, continuous D.C. mode operation for all values of current limiting resistance and throughout the voltage range (7 - 20 kV). The pulse mode and high frequency mode were rarely seen with this nozzle. The stability of this configuration for steady D.C. mode emission was demonstrated by the two life tests, which resulted in 15 hours and 25 hours of continuous D.C. emission. The current was a steady 35 μA at a power supply voltage of 11 kV and current limiting resistance of 100 MΩ.

A typical ion emission pattern is shown in Figure 33. At higher currents the pattern remained essentially the same size with the edges becoming slightly less sharply defined. The edges of the pattern correspond to a 18° emission half angle which results in 62 μA and 308 μA sr^{-1} for total currents of 20 μA and 100 μA respectively.

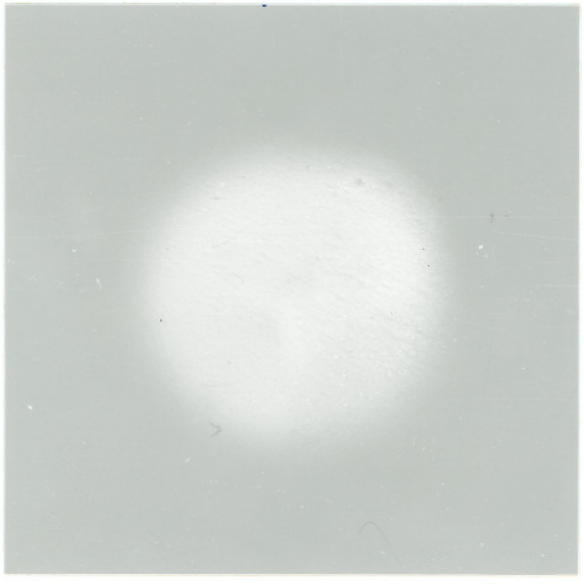

Fig. 33. Photograph of ion emission pattern.

DISCUSSION AND CONCLUSIONS

In both the electron and ion modes of operation a small point of incandescent light surrounded by a blue glow emanates from the tip of the Ga cone. This is an indication of localized heating and that electronic excitation of the Ga occurs during the emission process.

Two possible energy sources which could create the observed localized heating are the energy exchange processes attending field emission and the bombardment by secondary electrons during ion emission or by ions during electron emission. The first process, which has been studied previously,[11] causes the temperature of the tip T_o relative to the temperature T_1 at the base of the cone to vary according to

$$T_o - T_1 = \frac{kT \cot(\pi p)}{K}\left(\frac{I}{\alpha r}\right) + \frac{\rho(T)}{2K\pi^2}\left(\frac{I^2}{\alpha r}\right)^2 \qquad (29)$$

where K is the thermal conductivity, $\rho(T)$ is the electrical resistivity, r is the radius of the cone at the point of truncation and p is a dimensionless parameter which is a function of electric field and work function. The first term in Eq. (29) is due to the so-called "Nottingham heating" and the second term is due to resistive heating.[11] The plot of Eq. (29) in Figure 34 shows that in order to achieve sufficient heating to produce an incandescent glow that either

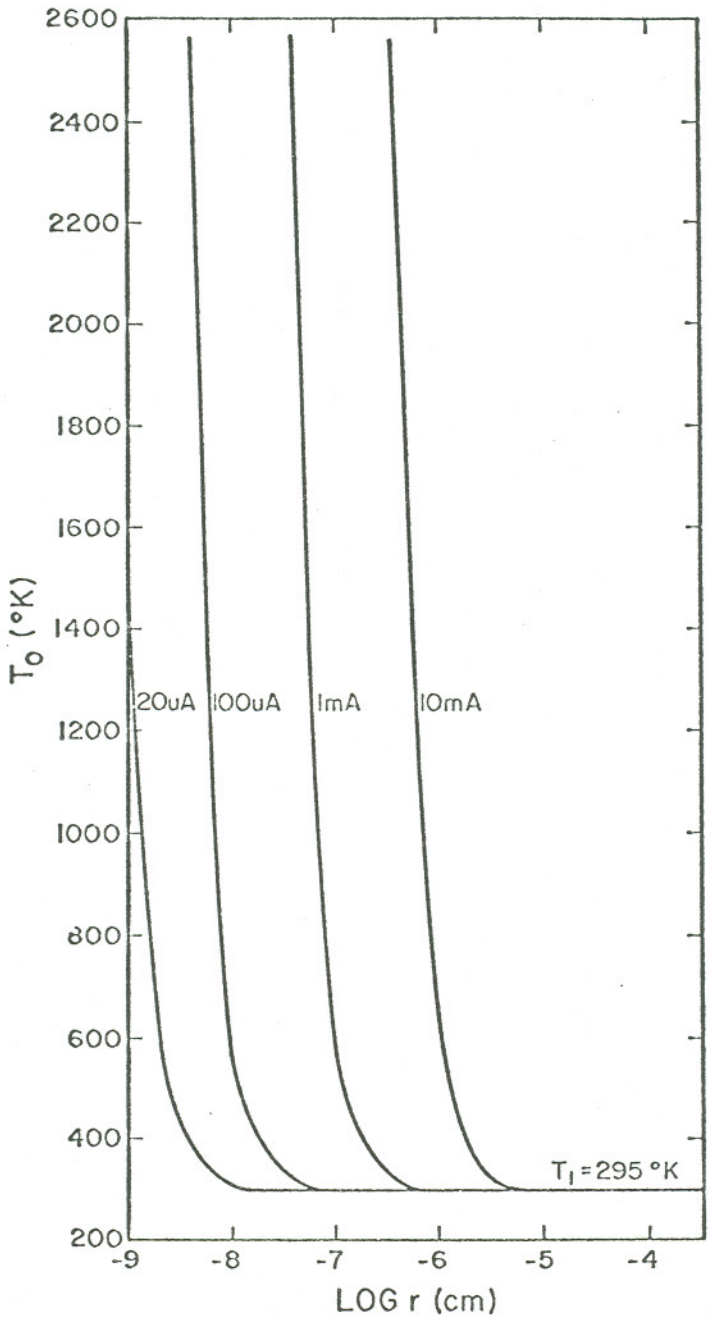

Figure 34. Apex temperature of a Ga cone due to heating by energy exchanges attending field emission vs apex radius.

relative large currents or a small radius is necessary.

Eq. (29) is the steady state or D.C. mode solution. For pulse mode, when the Nottingham effect is neglected and only resistive heating is considered, it has been shown[11] that T_o varies with pulse length, t_o, and pulse separation, t_1, according to the expression:

$$\left(T_o - T_1\right)_{\text{pulse}} = \left(T_o - T_1\right)_{DC} \left[\frac{\frac{2t_o}{t_c}}{1 + 2.63\sqrt{\frac{t_o}{t_c}} + \frac{2t_o}{t_c}} \right] \times \left[\frac{0.74}{1 + \frac{t_i}{t_c}\sqrt{2.2 + \frac{t_i}{t_c}}} \right] \tag{30}$$

where t_c is a time constant characteristic of the emitter material and cone - half angle:

$$t_c = \frac{c}{K\delta}\left(\frac{r_o}{\alpha}\right)^2 \tag{31}$$

where c is the specific heat and δ, the density of the emitter material.

The first bracket of Eq. (30) represents the effect of pulse length on T_o at the end of the pulse. For $t_o = t_c$ the tip temperature rise is 36% of the steady state value and for t_o appreciably larger than t_c, the tip is heated close to its steady state temperature. The second bracket represents the effect of repetition rate. If t_1 is

appreciably longer than t_c then almost complete cooling of the emitter tip occurs between pulses.

The Nottingham effect is ignored in the derivation of Eq. (30) in order to obtain an analytical solution. However, this effect causes the emitter tip to receive an additional input of energy localized at the tip, at a rate which decreases as tip temperature increases. Therefore it in effect reduces the time constant, t_c, below the value indicated by Eq. (31).

For a Ga cone of half angle 49.3°

$$t_c \approx 200\ r_o^2. \tag{32}$$

Then for Ga emission where t_o = 10 nanoseconds, $t_c = t_o$ when r_o = 707 Å and for r_o = 100 Å $t_c \approx 200\ t_o$. Thus for radii smaller than r_o = 100 Å $(T_o - T_1)$ pulse is close to the steady values of Eq. (29) and Figure 34. For these radii and t_c values, the measured and calculated values of t_1 obtained for Ga emission are such that $t_1 >> t_c$. Therefore complete emitter tip cooling should occur between pulses.

Thus, heating by this process is capable of producing the observed incandescent glow in either the steady state or pulse mode. However, based on the measured emission currents and short pulse length (small t_c value) it is necessary to have a relatively small (10 Å) radius in order to achieve sufficient heating.

Heating of the cone by electron or ion bombardment was shown by Clampitt[2] to vary according to

$$T_o - T_1 = \frac{IV}{K\pi\tan\theta}\left(\frac{1}{r_o} - \frac{1}{r_1}\right) \tag{33}$$

where I and V are the incident current and energy respectively and r_o and r_1 are the radii of the cone at T_o and T_1 respectively. Since usually $r_1 >> r_o$, the $1/r_1$ term can be ignored.

To achieve sufficient heating by this means, as shown by Figure 35, either a relatively large IV value or a small radius is necessary. A large IV value is easily obtained if the bombarding particles originate at or near the screen and thereby are accelerated by $\approx 10^4$ volts. However, these particles would strike the entire cone and result in unlocalized heating. Also, preliminary experiments in preferential biasing of the screen to eliminate particles originating at the screen from reaching to the emitter seem to produce no reduction in the localized heating. Thus it appears the incident particles must originate close to the cone meaning they possess only a few eV in energy and to achieve a large IV value necessitates a relatively large incident current. This seems feasible in the ion mode of operation but in the electron mode it seems unlikely to have as large incident ion current. Therefore, in order to create sufficient heating by this process a small radius is required.

The presence of the blue glow or excited Ga atoms in the space surrounding the cone is an unexpected result considering the very low vapor pressure of Ga. The vapor pressure, P, of a curved surface of radius, r, relative to a flat surface is given by[10]

$$\ell n \left(\frac{p}{p_o}\right) = \frac{2\gamma V_{in}}{RTr} \qquad (34)$$

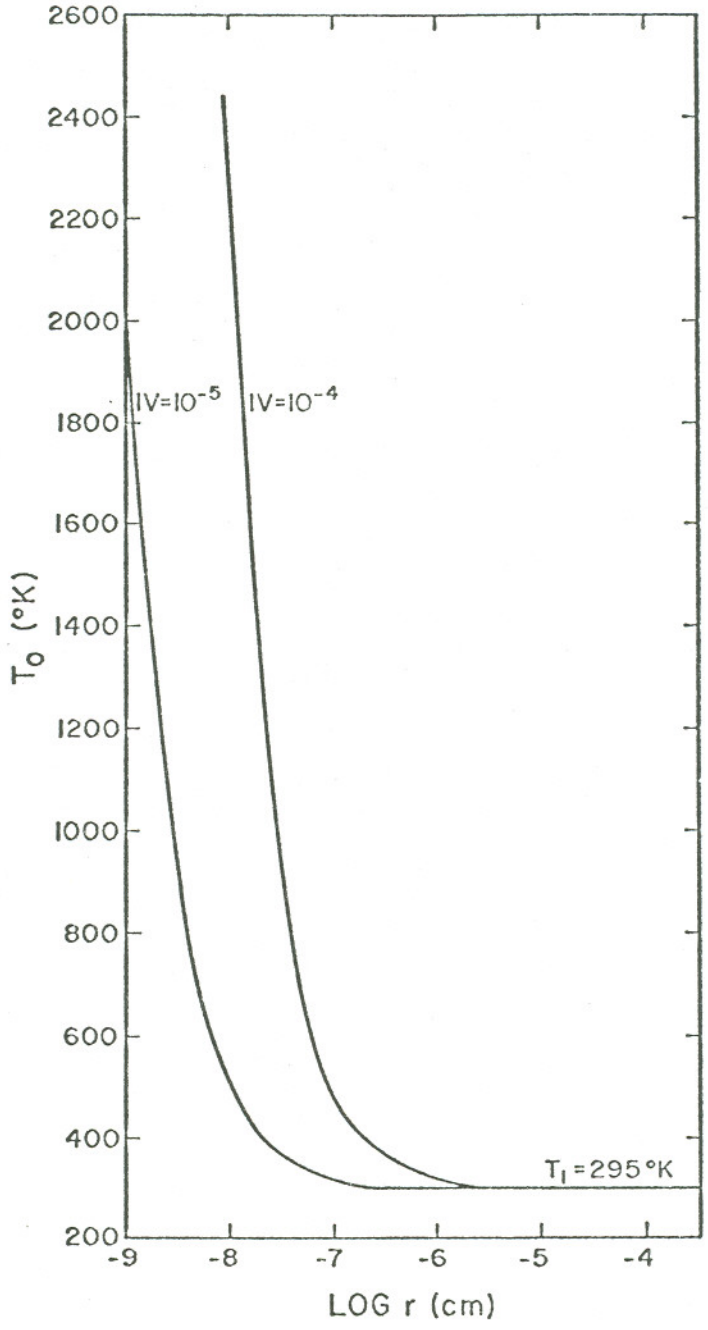

Figure 35. Apex temperature of a Ga cone due to heating by bombardment vs apex radius.

where V_{in} is the molar volume. Table VIII lists values of P for various radii and temperature and shows that the vapor pressure becomes large for radii less than ten Å.

TABLE VIII

Values of P/P_o for a Ga curved surface of radius r

$P_o = 10^{-8}$ torr at T = 825°K.

r (cm)	300°K	500°K	1000°K	2000°K
10^{-6}	2.0	1.5	1.2	1.1
10^{-7}	1×10^{3}	6×10^{1}	8.1	2.8
10^{-8}	1.6×10^{30}	1×10^{13}	1×10^{9}	3×10^{4}
10^{-9}	$> 10^{100}$	$> 10^{100}$	4×10^{90}	2×10^{45}

The incandescent and blue glow, material depletion, the high average and pulse currents indicate that the mechanism of electron emission is not purely a field emission process. From the fact that only a pulsed mode of operation has been observed with electron emission it is hypothesized that the electrostatic forces cause the liquid cone apex to approach a radius of a few atoms. This, in turn, leads to an increasing field and field emitted current. Accordingly, the cone is heated by electron-phonon energy exchanges increasing the tip temperature to an incandescent glow. The temperature and small radius increase the vapor pressure of the Ga until it is sufficiently high to form a plasma that vaporizes a small portion of the emitter and causes a large electron pulse to propagate across

the diode. Then, the apex of the liquid cone reforms and the process repeats.

A similar process occurs during the ion pulse mode of operation. However, the ion mode also exhibits a stable D.C. mode of operation. Apparently, under certain conditions, the cone apex radius is prevented from becoming extremely small by the simultaneous removal of material by field evaporation. A steady state condition is achieved where the cone is maintained at a constant apex radius by supplying material to the apex at a rate equal to its removal.

The mechanism of ion emission is not a pure field evaporation process as indicated by the incandescent and blue glow and high currents. It is more difficult to explain than the electron emission process and is not fully understood. However, it is hypothesized that the radius of the liquid cone apex becomes extremely small, $\simeq$ 10 Å. This results in field evaporation and an increase in the vapor pressure which releases neutral Ga atoms. As these atoms leave the tip they are gas phase ionized. The electrons bombard the apex and excite some of the releasing neutral atoms. This results in strong localized heating of the apex and further vaporization.

A space charge effect would seem possible with the high density of Ga ions surrounding the emitter. Such an effect would result in the current showing a dependence on the $V^{3/2}$ or $(V - V_T{}^{3/2})$, where V_T is threshold voltage. The I - V data collected thus far has not exhibited such a dependence and therefore shows no space charge effect.

SUMMARY

In summary, the liquid Ga field shows great promise as a high brightness and high current ion source. It appears capable of producing continuous high D.C. ion currents for long periods of time. The angular distribution is sharply defined and centered on the emitter's axis. Besides the D.C. mode, a pulse mode and high frequency mode were obtained in the ion mode of operation.

As an electron source the liquid field emitter exhibits only a pulse mode. It was characterized by a high amplitude pulse (40 - 100 Amps) of short duration (8 - 10 nanoseconds) with a two nanosecond rise time. The pulse rate governs the average current and increases with increasing voltage or decreasing load resistance. High average currents can be obtained and maintained. The angular distribution has a uniform intensity over an emitting half angle of greater than 40°.

Life tests in both ion and electron modes self-terminated when the liquid metal supply was exhausted. It appears that the source could emit indefinitely if an adequate supply of liquid metal was maintained at the needle's end.

Two key factors in obtaining stable emission are the ability of the liquid metal to wet the needle and having the proper amount of liquid metal at the needle's tip. Sufficient wetting was achieved

by argon sputtering or heat cleaning of the tip and adequate control over the position of the Ga meniscus was obtained by a gas pressure control system and long capillary tubing.

Emission from a localized cone formed on the end of an emitter was found to be more stable than emission from an unsupported cone. The unsupported liquid metal forms a cone approximately Taylor's theoretical half angle of 49.3°. It has a higher threshold voltage and emits higher currents for a given voltage-load resistor combination than the inserted emitter designs. The W-3 source configuration produced the most stable emission and longest continuous emission.

The emission mechanism appears to not be a pure field emission or field evaporation process, but rather a complex process which is probably initiated by the former processes. The most distinctive feature of the process is an incandescent and blue glow indicating localized heating and presence of excited Ga atoms in space surrounding the cone.

It is possible that reliable and consistent liquid metal ion or electron source can be made. However, more experimental and theoretical work is necessary to find the optimum source configuration. Some of the experimental parameters to be studied in the future include the cone angle, apex radius, shank radius, and protruding distance of the inserted emitter of the source design of W-3. Also, a smaller nozzle size should provide more stable

emission from unsupported Taylor cones. To better understand the emission a spectral analysis of the radiated light, pyrometer temperature measurements, and high magnification photographs of the emitting site should provide valuable information.

REFERENCES

1. V. E. Krohn and G. R. Ringo, Appl. Phys. Letters 27, 479 (1975).

2. R. Clampitt, K. L. Aitken, D. K. Jefferies, ESTEC Contract Report 2050/73 (1975).

3. J. F. Mahoney, A. T. Yahiku, H. L. Daley, R. D. Moore and J. Perel, J. Appl. Phys. 40, 5101 (1969).

4. D. S. Swatik and C. D. Hendricks, AIAA J. 6, 1596 (1968).

5. G. Taylor, Proc. Roy. Soc. (London) A280, 383 (1964).

6. E. E. Martin, F. M. Charbonnier, W. W. Dolan, W. P. Dyke, H. W. Pitman, J. K. Trolan, Wadd Techn. Report 59-20 (1960).

7. B. W. Colby and C. A. Evans, Jr., Anal. Chem. 45, 1887 (1973).

8. L. R. Kelman, W. D. Wilkinson, F. L. Yaggee, Resistance of Materials to Attack by Liquid Metals, Argonne Natl. Lab. 4417 (1950).

9. G. A. Somorjai, Principles of Surface Chemistry, Prentice-Hall Inc., New Jersey (1972).

10. M. Green, Solid State Surface Science, Marcel Dekker, New York (1973).

11. L. W. Swanson, L. C. Crouser and F. M. Charbonnier, Phys. Rev. 151, 327 (1966).

APPENDIX I

Eq.(22) is easily obtained by direct application of the difference equation to Laplace's equation in cylindrical coordinates, Eq.(21). To derive Eq.(23), one first considers Laplace's equation in cartesian coordinates,

$$\frac{\partial^2\phi}{\partial x^2} + \frac{\partial^2\phi}{\partial y^2} + \frac{\partial^2\phi}{\partial z^2} = 0 \tag{35}$$

Application of the difference equation to the above yields,

$$\phi(x + h,y,z) + \phi(x - h,y,z) + \phi(x,y + h,z) + \phi(x, y-h,z)$$
$$+ \phi(x,y,z + h) + \phi(x,y,z - h) - 6\ \phi(x,y,z) + O(h^4) = 0. \tag{36}$$

For a point on the z-axis, assuming azimuthal symmetry and converting to cylindrical coordinates, then Eq.(36) becomes,

$$4\ \phi(h,z) + \phi(0,z + h) + \phi(0, z-h) - 6\ \phi(0,z) + O(h^4) = 0 \tag{37}$$

which is equivalent to Eq.(23).

Four computer programs (POT1, POT2, Subroutine BC, EQUI) were used to calculate equipotential lines for various source and high voltage extractor configurations. POT1 used Equations (22) and (23) and a standard iterative procedure, with a step size of 3.75 mils, to calculate the potential at each interior point of a 70 × 50 matrix. The nozzle was set at zero potential and the high voltage extractor at V_o (usually V_o = 7 kV). The remaining boundary conditions and initial values of the interior points were calculated

by subroutine BC based on well-known equations for the potential at a point due to a solid circular ring possessing a constant charge density.

POT2 used the same method as POT1 to calculate the potential of the interior points of a 100 × 50 matrix with a step size of 0.375 mils. The boundary conditions were obtained using linear interpolation on the results from POT1, specifically rows 15 and 26, and column 5.

Program EQUI used linear interpolation on the results from POT1 and POT2 to calculate the coordinates of the equipotential line for any specified potential. The equipotential lines were then plotted with typical results shown in Figure 2.

```
C      POTENTIAL PROGRAM POT1


C      POTENTIAL PROGRAM POT1
       DIMENSION V(50,70)
       COMMON PALPH(12),KQ(3),P1,I,J,RADL,RADS
       CALL SEARCH(2,'TRAILB',1,0)
       READ(1,285)P1,R
  285  FORMAT(F6.0,F8.2)
       READ(1,300)K1,N
  300  FORMAT(I2,I2)
       WRITE(1,707)P1,R,K1,N
  707  FORMAT('P1=',F9.2,5X,'R=',F9.2,5X,'I=',I2,5X,
     C'J=',I2)
       DIA=4.
       RADS=DIA/2.
       RADL=K1+RADS
       DO 3 L=1,3
     3 KQ(L)=1
       APP=N+RADS
       K=0
       M=DIA+N
       K2=K1+DIA
       DO 5 I=1,50
       DO 5 J=1,70
       IF(I+J.EQ.2) GO TO 5
       CALL BC(APP,PHI)
       V(I,J)=PHI
     5 CONTINUE
       DO 10 J=N,M
       DO 10 I=K1,K2
    10 V(I,J)=1.0
       DO 15 J=1,21
    15 V(1,J)=1.0
       DO 52 I=1,21
    52 V(2,I)=0
       V(1,22)=0
       DO 54 I=K1,K2
       V(I,N)=P1
    54 V(I,M)=P1
       DO 60 J=N,M
       V(K1,J)=P1
    60 V(K2,J)=P1
     1 S=0
       K=K+1
       DO 69 J=23,69
```

```
      D=((V(1,J+1)+4*V(2,J)+V(1,J-1))/6)-V(1,J)
      S=S+ABS(D)
   69 V(1,J)=V(1,J)+D
      KR=3
      DO 70 J=2,22
      IF(J.EQ.22.) KR=2
      DO 70 I=KR,49
      D=.25*(V(I,J+1)+V(I,J-1)+V(I+1,J)+V(I-1,J))
      D=D+(1/(8*(I-1)))*(V(I+1,J)-V(I-1,J))-V(I,J)
      S=S+ABS(D)
   70 V(I,J)=V(I,J)+D
      DO 72 J=23,69
      IF(J.EQ.M) GO TO 700

   71 DO 72 I=2,49
      D=.25*(V(I,J+1)+V(I,J-1)+V(I+1,J)+V(I-1,J))
      D=D+(1/(8*(I-1)))*(V(I+1,J)-V(I-1,J))-V(I,J)
      S=S+ABS(D)

   72 V(I,J)=V(I,J)+D
      KP=1
      KF=2
      KR=K1-1
   76 DO 74 J=M,M
      DO 74 I=KF,KR
      D=.25*(V(I,J+1)+V(I,J-1)+V(I+1,J)+V(I-1,J))
      D=D+(1/(8*(I-1)))*(V(I+1,J)-V(I-1,J))-V(I,J)
      S=S+ABS(D)
      V(I,J)=V(I,J)+D
   74 IF(J.EQ.M) GO TO 800
  800 KF=K2+1
      KR=49
      IF(KP.EQ.5) GO TO 75
      KP=5.0
      GO TO 76
   75 WRITE(1,203)S
      IF(S.GT.R) GO TO 1
      WRITE(1,200)K
      L=1
      L1=8
      DO 91 LN=1,6
      DO 90 J=1,70
   90 WRITE(5,201)(V(I,J), I=L,L1)
      L=LN*8+1
   91 L1=L+7
      GO TO 701
```

```
700  J=M+1
     GO TO 71
701  CONTINUE
     CALL SEARCH(4,0,1,0)
201  FORMAT(8(F9.2))
200  FORMAT(1H1,10X,'NUMBER OF ITERATIONS',I5)
203  FORMAT(10X,F10.4)
     CALL EXIT
     END
     SUBROUTINE BC(CIJ,PHI)
     DIMENSION X(12),P(12)
     COMMON PALPH(12),KQ(3),P1,I,J,RADL,RADS
     CON=.0001985
     A=RADL*CON
     B=RADS*CON
     IF(KQ(2).EQ.1) GO TO 800
   4 FCJ=(CIJ-1)*CON
     FJ=(J-1)*CON
     FI=(I-1)*CON
     KQ(3)=KQ(3)+1
     IF(KQ(3).EQ.2) GO TO 21
   5 IF(KQ(2).GT.1) GO TO 6
  21 COSA=(FCJ)/((A*A+(FCJ)**2.)**.5)
     Y=COSA

     KQ(2)=3
     GO TO 9
   6 R=(FJ**2.+FI**2.)**.5
     C=(A*A+(FCJ)**2.)**.5
     IF(R-C)30,32,32
  30 BIG=C
     SM=R
     GO TO 8
  32 BIG=R
     SM=C
   8 Y=FJ/R
   9 DO 10 M=1,12
  10 X(M)=Y**M
     P(1)=X(1)
     P(2)=(1./2 )*(3*X(2)-1)
     P(3)=(1./2 )*(5*X(3)-3*X(1))
     P(4)=(1./8.)*(35*X(4)-30*X(2)+3)
     P(5)=(1./8.)*(63*X(5)-70*X(3)+15*X(1))
     P(6)=(1./16.)*(231*X(6)-315*X(4)+105*X(2)-5)
     P(7)=(1./16.)*(429*X(7)-693*X(5)+315*X(3)-35*
    CX(1))
     P(8)=(1./128.)*(6435*X(8)-12012*X(6)+6930*X(4)
```

```
     C-1260*X(2)+35)
      P(9)=(1./128.)*(12155*X(9)-25740.*X(7)+18018.
     C*X(5)-4620.*X(3)+315*X(1))
      P(10)=(1./256.)*(46189.*X(10)-109395.*X(8)
     C+98098.*X(6)-38038.*X(4)+3465.*X(2)-63)
      P(11)=(1./256.)*(88179.*X(11)-230945.*X(9)+
     C218790.*X(7)-98098.*X(5)+15015.*X(3)-693.*X(1))
      P(12)=(1./1024.)*(676039.*X(12)-1939938.*X(10)
     C+2078505.*X(8)-1021020.*X(6)+225225.*X(4)-18018.
     C*X(2)+231)
      IF(K0(2).EQ.3) GO TO 900
      SUM=0
      DO 20 M=1,12
   20 SUM=SUM+((1./BIG)*((SM/BIG)**M))*PALPH(M)*P(M)
  500 FORMAT(3(5X,F9.2))
      PHI=K0(1)*((1./BIG)+SUM)
      IF(K0(3).EQ.2) GO TO 850
      IF(K0(2).EQ.7) GO TO 901
      K0(1)=(P1*(B/((A*A+B*B)**.5)))/PHI
  707 FORMAT(4(E15.5,3X))
      K0(2)=7
      GO TO 4
  900 DO 50 M=1,12
   50 PALPH(M)=P(M)
      K0(2)=5
      GO TO 5
  800 FCJ=5.*CON
      FJ=FCJ
      FI=0.
      GO TO 5
  850 K0(2)=7
  901 RETURN
      END
```

```
      CALL SEARCH(1,"TRAILB",1,0)
      CALL SEARCH(2,"DASFFF",2,0)
      READ(1,203)R
  203 FORMAT(F9.2)
      DO 5 K=1,26
    5 READ(5,207)(V(I,K), I=1,6)
      DO 6 J=16,26
      DO 6 I=1,5
      S=(V(I+1,J)-V(I,J))/10
      DO 6 L=1,10
      K=((I-1)*10)+L
      N=((J-16)*18)+1
      P(K,N)=(S*(L-1))+V(I,J)
      IF(N.EQ.181) GO TO 6
      DO 6 M=1,9
      MM=N+M
    6 P(K,MM)=P(K,N)
      DO 7 I=16,25
```

```
 21 P(I,J)=P(I,J)+D
    DO 22 J=47,61
    N=63-J
    DO 22 I=N,50
    D=.25*(P(I,J+1)+P(I,J-1)+P(I+1,J)+P(I-1,J))
    D=D+(1/(8*(I-1)))*(P(I+1,J)-P(I-1,J))-P(I,J)
    S=S+ABS(D)
 22 P(I,J)=P(I,J)+D
    DO 23 J=2,46
    DO 23 I=17,50
    D=.25*(P(I,J+1)+P(I,J-1)+P(I+1,J)+P(I-1,J))
    D=D+(1/(8*(I-1)))*(P(I+1,J)-P(I-1,J))-P(I,J)
    S=S+ABS(D)
 23 P(I,J)=P(I,J)+D

    WRITE(1,204)S
204 FORMAT(10X,F10.2)
    IF(S.GT.R) GO TO 1
    DO 25 I=1,50
    DO 25 J=1,100
 25 IF(P(I,J).EQ.V(1,26)/2) P(I,J)=1
    L=1
    L1=8
    DO 30 LN=1,6
    DO 31 J=1,101
 31 WRITE(6,201)(P(I,J), I=L,L1)
    L=LN*8+1
 30 L1=L+7
207 FORMAT(6(F9.2))
    CALL SEARCH(4,0,1,0)
    CALL SEARCH(4,0,2,0)
201 FORMAT(8(F9.2))
    CALL EXIT
    END
```

```
C       PROGRAM EQUI


C       PROGRAM EQUI
        DIMENSION V(50,101),X(8)
        CALL SEARCH(1,'TRAILB',1,0)
        J=0
        L=0
        READ(1,204)MJ,MR
        DO 5 K=1,MR
        READ(5,205)(X(I),I=1,8)
        J=J+1
        DO 6 M=1,8
        N=(8*L)+M
    6   V(N,J)=X(M)
        IF(J.EQ.MJ) GO TO 700
        GO TO 5
  700   J=0
        L=L+1
    5   CONTINUE
  205   FORMAT(8(F9.2))
        READ(1,200)KM
        DO 2 K=1,KM
        READ(1,201)N,N1,M,M1,P1
        WRITE(4,203)N,N1,M,M1,P1
        DO 2 I=N,N1
        DO 2 J=M,M1
        IF(V(I,J).EQ.P1) GO TO 101
        IF(V(I,J).GT.P1.AND.V(I,J+1).LT.P1) GO TO 50
        IF(V(I,J+1).GT.P1.AND.V(I,J).LT.P1) GO TO 50
        GO TO 2
   50   Z=((P1-V(I,J))/(V(I,J+1)-V(I,J)))+(J-1)
        GO TO 8
  101   Z=J-1
    8   LN=I-1
        WRITE(4,202)LN,Z
    2   CONTINUE
  200   FORMAT(I2)
  201   FORMAT(4(I3),F6.0)
  202   FORMAT(1H ,10X,I3,10X,F8.3)
  203   FORMAT(1H0,/,8X,2(I3,2X,I3,10X),F6.0)
  204   FORMAT(I4,I4)
        CALL EXIT
        END
```

VITA

The author was born April 24, 1952 in Billings, Montana. His public school education began in Billings and was continued in San Carlos, California and was culminated in Portland, Oregon when he graduated as an Oregon Scholar from Sunset High School in 1970. He then attended Willamette University and graduated in May, 1974 with a Bachelor of Arts degree in Mathematics and Physics. In September, 1974 he began his graduate studies at the Oregon Graduate Center. Doing his thesis work under the direction of Dr. Lynwood Swanson, the requirements for a Master of Science degree in Physics were completed in March, 1977.